LATTICE BOLTZMANN METHOD FOR FLUID FLOWS

Shiyi Chen[1,2] *and Gary D. Doolen*[2]

[1]IBM Research Division, T. J. Watson Research Center, P.O. Box 218, Yorktown Heights, NY 10598; [2]Theoretical Division and Center for Nonlinear Studies, Los Alamos National Laboratory, Los Alamos, NM 87545; e-mail: syc@cnls.lanl.gov

KEY WORDS: lattice Boltzmann method, mesoscopic approach, fluid flow simulation

ABSTRACT

We present an overview of the lattice Boltzmann method (LBM), a parallel and efficient algorithm for simulating single-phase and multiphase fluid flows and for incorporating additional physical complexities. The LBM is especially useful for modeling complicated boundary conditions and multiphase interfaces. Recent extensions of this method are described, including simulations of fluid turbulence, suspension flows, and reaction diffusion systems.

INTRODUCTION

In recent years, the lattice Boltzmann method (LBM) has developed into an alternative and promising numerical scheme for simulating fluid flows and modeling physics in fluids. The scheme is particularly successful in fluid flow applications involving interfacial dynamics and complex boundaries. Unlike conventional numerical schemes based on discretizations of macroscopic continuum equations, the lattice Boltzmann method is based on microscopic models and mesoscopic kinetic equations. The fundamental idea of the LBM is to construct simplified kinetic models that incorporate the essential physics of microscopic or mesoscopic processes so that the macroscopic averaged properties obey the desired macroscopic equations. The basic premise for using these simplified kinetic-type methods for macroscopic fluid flows is that the macroscopic dynamics of a fluid is the result of the collective behavior of many microscopic particles in the system and that the macroscopic dynamics is not sensitive to the underlying details in microscopic physics (Kadanoff 1986). By developing a simplified version of the kinetic equation, one avoids solving

329

complicated kinetic equations such as the full Boltzmann equation, and one avoids following each particle as in molecular dynamics simulations.

Even though the LBM is based on a particle picture, its principal focus is the averaged macroscopic behavior. The kinetic equation provides many of the advantages of molecular dynamics, including clear physical pictures, easy implementation of boundary conditions, and fully parallel algorithms. Because of the availability of very fast and massively parallel machines, there is a current trend to use codes that can exploit the intrinsic features of parallelism. The LBM fulfills these requirements in a straightforward manner.

The kinetic nature of the LBM introduces three important features that distinguish it from other numerical methods. First, the convection operator (or streaming process) of the LBM in phase space (or velocity space) is linear. This feature is borrowed from kinetic theory and contrasts with the nonlinear convection terms in other approaches that use a macroscopic representation. Simple convection combined with a relaxation process (or collision operator) allows the recovery of the nonlinear macroscopic advection through multi-scale expansions. Second, the incompressible Navier-Stokes (NS) equations can be obtained in the nearly incompressible limit of the LBM. The pressure of the LBM is calculated using an equation of state. In contrast, in the direct numerical simulation of the incompressible NS equations, the pressure satisfies a Poisson equation with velocity strains acting as sources. Solving this equation for the pressure often produces numerical difficulties requiring special treatment, such as iteration or relaxation. Third, the LBM utilizes a minimal set of velocities in phase space. In the traditional kinetic theory with the Maxwell-Boltzmann equilibrium distribution, the phase space is a complete functional space. The averaging process involves information from the whole velocity phase space. Because only one or two speeds and a few moving directions are used in LBM, the transformation relating the microscopic distribution function and macroscopic quantities is greatly simplified and consists of simple arithmetic calculations.

The LBM originated from lattice gas (LG) automata, a discrete particle kinetics utilizing a discrete lattice and discrete time. The LBM can also be viewed as a special finite difference scheme for the kinetic equation of the discrete-velocity distribution function. The idea of using the simplified kinetic equation with a single-particle speed to simulate fluid flows was employed by Broadwell (Broadwell 1964) for studying shock structures. In fact, one can view the Broadwell model as a simple one-dimensional lattice Boltzmann equation. Multispeed discrete particle velocities models have also been used for studying shock-wave structures (Inamuro & Sturtevant 1990). In all these models, although the particle velocity in the distribution function was discretized, space and time were continuous. The full discrete particle velocity model, where

space and time are also discretized on a square lattice, was proposed by Hardy et al (1976) for studying transport properties of fluids. In the seminal work of the lattice gas automaton method for two-dimensional hydrodynamics, Frisch et al (1986) recognized the importance of the symmetry of the lattice for the recovery of the Navier-Stokes equation; for the first time they obtained the correct Navier-Stokes equation starting from the lattice gas automata on a hexagonal lattice. The central ideas in the papers contemporary with the FHP paper include the cellular automaton model (Wolfram 1986) and the 3-D model using the four-dimensional face-centered-hyper-cubic (FCHC) lattice (d'Humières et al 1986).

The lattice gas automaton is constructed as a simplified, fictitious molecular dynamic in which space, time, and particle velocities are all discrete. From this perspective, the lattice gas method is often called lattice gas cellular automata. In general, a lattice gas automaton consists of a regular lattice with particles residing on the nodes. A set of Boolean variables $n_i(\mathbf{x}, t)(i = 1, \cdots, M)$ describing the particle occupation is defined, where M is the number of directions of the particle velocities at each node. The evolution equation of the LG automata is as follows:

$$n_i(\mathbf{x} + \mathbf{e}_i, t + 1) = n_i(\mathbf{x}, t) + \Omega_i(n(\mathbf{x}, t)), \qquad (i = 0, 1 \cdots, M), \quad (1)$$

where $\mathbf{e}_i$ are the local particle velocities. Starting from an initial state, the configuration of particles at each time step evolves in two sequential sub-steps, (*a*) streaming, in which each particle moves to the nearest node in the direction of its velocity, and (*b*) collision, which occurs when particles arriving at a node interact and change their velocity directions according to scattering rules. For simplicity, the exclusion principle (no more than one particle being allowed at a given time and node with a given velocity) is imposed for memory efficiency and leads to a Fermi-Dirac local equilibrium distribution (Frisch et al 1987).

The main feature of the LBM is to replace the particle occupation variables, n_i (Boolean variables), in Equation 1 by single-particle distribution functions (real variables) $f_i = \langle n_i \rangle$ and neglect individual particle motion and particle-particle correlations in the kinetic equations (McNamara & Zanetti 1988), where $\langle \ \rangle$ denotes an ensemble average. This procedure eliminates statistical noise in the LBM. In the LBM, the primitive variables are the averaged particle distributions, which are mesoscopic variables. Because the kinetic form is still the same as the LG automata, the advantages of locality in the kinetic approach are retained. The locality is essential to parallelism.

An important simplification of the LBM was made by Higuera & Jiménez (1989) who linearized the collision operator by assuming that the distribution is close to the local equilibrium state. An enhanced collision operator approach which is linearly stable was proposed by Higuera et al (1989). A particular

simple linearized version of the collision operator makes use of a relaxation time towards the local equilibrium using a single time relaxation. The relaxation term is known as the Bhatnagar-Gross-Krook (BGK) collision operator (Bhatnagar et al 1954) and has been independently suggested by several authors (Qian 1990, Chen et al 1991). In this lattice BGK (LBGK) model, the local equilibrium distribution is chosen to recover the Navier-Stokes macroscopic equations (Qian et al 1992, Chen et al 1992). Use of the lattice BGK model makes the computations more efficient and allows flexibility of the transport coefficients.

LATTICE BOLTZMANN EQUATIONS

LBE: An Extension of LG Automata

There are several ways to obtain the lattice Boltzmann equation (LBE) from either discrete velocity models or the Boltzmann kinetic equation. There are also several ways to derive the macroscopic Navier-Stokes equations from the LBE. Because the LBM is a derivative of the LG method, we will introduce the LBE beginning from a discrete kinetic equation for the particle distribution function, which is similar to the kinetic equation in the LG automata in Equation 1:

$$f_i(\mathbf{x} + \mathbf{e}_i \Delta x, t + \Delta t) = f_i(\mathbf{x}, t) + \Omega_i(f(\mathbf{x}, t)), \quad (i = 0, 1 \cdots, M), \quad (2)$$

where f_i is the particle velocity distribution function along the ith direction; $\Omega_i = \Omega_i(f(\mathbf{x}, t))$ is the collision operator which represents the rate of change of f_i resulting from collision. Δt and Δx are time and space increments, respectively. When $\Delta x / \Delta t = |\mathbf{e}_i|$, Equations 1 and 2 have the same discretizations. Ω_i depends only on the local distribution function. In the LBM, space is discretized in a way that is consistent with the kinetic equation, i.e. the coordinates of the nearest neighbor points around $\mathbf{x}$ are $\mathbf{x} + \mathbf{e}_i$.

The density ρ and momentum density $\rho \mathbf{u}$ are defined as particle velocity moments of the distribution function, f_i,

$$\rho = \sum_i f_i, \qquad \rho \mathbf{u} = \sum_i f_i \mathbf{e}_i, \qquad (3)$$

where $\sum_i \equiv \sum_{i=1}^{M}$. Ω_i is required to satisfy conservation of total mass and total momentum at each lattice:

$$\sum_i \Omega_i = 0, \qquad \sum_i \Omega_i \mathbf{e}_i = 0. \qquad (4)$$

If only the physics in the long-wave–length and low-frequency limit are of interest, the lattice spacing Δx and the time increment Δt in Equation 2 can be regarded as small parameters of the same order ε. Performing a Taylor

expansion in time and space, we obtain the following continuum form of the kinetic equation accurate to second order in ε:

$$\frac{\partial f_i}{\partial t} + \mathbf{e}_i \cdot \nabla f_i + \varepsilon \left(\frac{1}{2} \mathbf{e}_i \mathbf{e}_i : \nabla \nabla f_i + \mathbf{e}_i \cdot \nabla \frac{\partial f_i}{\partial t} + \frac{1}{2} \frac{\partial^2 f_i}{\partial t^2} \right) = \frac{\Omega_i}{\varepsilon}. \tag{5}$$

To derive the macroscopic hydrodynamic equation, we employ the Chapman-Enskog expansion, which is essentially a formal multiscaling expansion (Frisch et al 1987),

$$\left[\frac{\partial}{\partial t} = \varepsilon \frac{\partial}{\partial t_1} + \varepsilon^2 \frac{\partial}{\partial t_2}, \qquad \frac{\partial}{\partial x} = \varepsilon \frac{\partial}{\partial x_1}. \right]$$

The above formula assumes that the diffusion time scale t_2 is much slower than the convection time scale t_1. Likewise, the one-particle distribution function f_i can be expanded formally about the local equilibrium distribution function f_i^{eq},

$$f_i = f_i^{eq} + \varepsilon f_i^{(neq)}. \tag{6}$$

Here f_i^{eq} depends on the local macroscopic variables (ρ and $\rho \mathbf{u}$) and should satisfy the following constraints:

$$\sum_i f_i^{eq} = \rho, \qquad \sum_i f_i^{eq} \mathbf{e}_i = \rho \mathbf{u}. \tag{7}$$

$f_i^{(neq)} = f_i^{(1)} + \varepsilon f_i^{(2)} + O(\varepsilon^2)$ is the nonequilibrium distribution function, which has the following constraints:

$$\sum_i f_i^{(k)} = 0, \qquad \sum_i f_i^{(k)} \mathbf{e}_i = 0, \tag{8}$$

for both $k = 1$ and $k = 2$.

Inserting f_i into the collision operator Ω_i, the Taylor expansion gives:

$$\Omega_i(f) = \Omega_i(f^{eq}) + \epsilon \frac{\partial \Omega_i(f^{eq})}{\partial f_j} f_j^{(1)}$$

$$+ \epsilon^2 \left(\frac{\partial \Omega_i(f^{eq})}{\partial f_j} f_j^{(2)} + \frac{\partial^2 \Omega_i(f^{eq})}{\partial f_j \partial f_k} f_j^{(1)} f_k^{(1)} \right) + O(\varepsilon^3). \tag{9}$$

From Equation 5, we note that when $\varepsilon \to 0$, we have: $\Omega_i(f^{eq}) = 0$. This leads to a linearized collision operator,

$$\frac{\Omega_i(f)}{\varepsilon} = \frac{M_{ij}}{\varepsilon} \left(f_j - f_j^{eq} \right), \tag{10}$$

where $M_{ij} \equiv \frac{\partial \Omega_i(f^{eq})}{\partial f_j}$ is the collision matrix (Higuera & Jiménez 1989), which determines the scattering rate between directions i and j. For a given lattice,

M_{ij} only depends on the angle between directions i and j and has a limited set of values. For mass and momentum conservation collision, M_{ij} satisfy the following constraints (Benzi et al 1992):

$$\sum_{i=1}^{M} M_{ij} = 0, \qquad \sum_{i=1}^{M} \mathbf{e}_i M_{ij} = 0. \tag{11}$$

If we further assume that the local particle distribution relaxes to an equilibrium state at a single rate τ,

$$M_{ij} = -\frac{1}{\tau}\delta_{ij}, \tag{12}$$

we arrive at the lattice BGK collision term (Bhatnagar et al 1954),

$$\frac{\Omega_i}{\varepsilon} = -\frac{1}{\tau} f_i^{neq} = -\frac{1}{\varepsilon\tau}\left(f_i^{(1)} + \varepsilon f_i^{(2)}\right), \tag{13}$$

and the LBGK equation:

$$f_i(\mathbf{x} + \mathbf{e}_i, t + 1) = f_i(\mathbf{x}, t) - \frac{f_i - f_i^{eq}}{\tau}. \tag{14}$$

The BGK collision term (Qian 1990, Chen et al 1991, Qian et al 1992, Chen et al 1992) was used previously in the full Boltzmann simulation for studying shock formation (Chu 1965) and was used recently for a shock-capturing using finite-volume methods (Xu & Prendergast). From Equation 5 one obtains the following equations:

$$\frac{\partial f_i^{eq}}{\partial t_1} + \mathbf{e}_i \cdot \nabla_1 f_i^{eq} = -\frac{f_i^{(1)}}{\tau}, \tag{15}$$

to order ε^0 and

$$\frac{\partial}{\partial t_1} f_i^{(1)} + \frac{\partial}{\partial t_2} f_i^{eq} + \mathbf{e}_i \cdot \boldsymbol{\nabla} f_i^{(1)} + \frac{1}{2}\mathbf{e}_i\mathbf{e}_i : \boldsymbol{\nabla}\boldsymbol{\nabla} f_i^{eq}$$
$$+ \mathbf{e}_i \cdot \boldsymbol{\nabla}\frac{\partial}{\partial t_1} f_i^{eq} + \frac{1}{2}\frac{\partial^2}{\partial t_1^2} f_i^{eq} = \frac{1}{\tau} f_i^{(2)}, \tag{16}$$

to order ε^1. Using Equation 15 and some algebra, we can rewrite the first order equation as

$$\frac{\partial f_i^{(1)}}{\partial t_2} + \left(1 - \frac{2}{\tau}\right)\left[\frac{\partial f_i^{(1)}}{\partial t_1} + \mathbf{e}_i \cdot \nabla_1 f_i^{(1)}\right] = -\frac{f_i^{(2)}}{\tau}. \tag{17}$$

From Equations 15 and 17 we obtain the following mass and momentum equations:

$$\frac{\partial \rho}{\partial t} + \nabla \cdot \rho\mathbf{u} = 0, \tag{18}$$

$$\frac{\partial \rho \mathbf{u}}{\partial t} + \nabla \cdot \Pi = 0, \tag{19}$$

which are accurate to second order in ε for Equation 2. Here the momentum flux tensor Π has the form:

$$\Pi_{\alpha\beta} = \sum_i (\mathbf{e}_i)_\alpha (\mathbf{e}_i)_\beta \left[f_i^{eq} + \left(1 - \frac{1}{2\tau}\right) f_i^{(1)} \right], \tag{20}$$

and $(\mathbf{e}_i)_\alpha$ is the component of the velocity vector $\mathbf{e}_i$ in the α-coordinate direction.

To specify the detailed form of $\Pi_{\alpha\beta}$, the lattice structure and the corresponding equilibrium distribution have to be specified. For simplicity and without loss of generality, we consider here the two-dimensional square lattice with nine velocities: $\mathbf{e}_i = (cos(\pi/2(i-1)), sin(\pi/2(i-1)))$ for $i = 1, 3, 5, 7$, $\mathbf{e}_i = \sqrt{2}(cos(\pi/2(i-1) + \pi/4, sin(\pi/2(i-1) + \pi/4))$ for $i = 2, 4, 6, 8$; $\mathbf{e}_0 = 0$ corresponds to a zero-speed velocity. The requirement for using the nine-velocity model, instead of the simpler five-velocity square lattice, comes from the consideration of lattice symmetry: the LBE cannot recover the correct Navier-Stokes equations unless sufficient lattice symmetry is guaranteed (Frisch et al 1986).

Note that the Navier-Stokes equations has a second-order nonlinearity. The general form of the equilibrium distribution function can be written up to $O(u^2)$ (Chen et al 1992):

$$f_i^{eq} = \rho \left[a + b\mathbf{e}_i \cdot \mathbf{u} + c(\mathbf{e}_i \cdot \mathbf{u})^2 + du^2 \right], \tag{21}$$

where a, b, c and d are lattice constants. This expansion is valid only for small velocities, or small Mach numbers u/C_s, where C_s is the sound speed. Using the constraints in Equation 7, the coefficients in Equation 21 can be obtained analytically (Qian et al 1992):

$$f_i^{\text{eq}} = \rho w_i \left[1 + 3\mathbf{e}_i \cdot \mathbf{u} + \frac{9}{2}(\mathbf{e}_i \cdot \mathbf{u})^2 - \frac{3}{2}u^2 \right], \tag{22}$$

with $w_0 = 4/9$, $w_1 = w_3 = w_5 = w_7 = 1/9$, and $w_2 = w_4 = w_6 = w_8 = 1/36$. Inserting the above formula into Equation 20 we have,

$$\Pi_{\alpha\beta}^{(0)} = \sum_i (\mathbf{e}_i)_\alpha (\mathbf{e}_i)_\beta f_i^{eq} = p\delta_{\alpha\beta} + \rho u_\alpha u_\beta,$$

$$\Pi_{\alpha\beta}^{(1)} = \left(1 - \frac{1}{2\tau}\right) \sum_i (\mathbf{e}_i)_\alpha (\mathbf{e}_i)_\beta f_i^1 = \nu(\nabla_\alpha(\rho\mathbf{u}_\beta) + \nabla_\beta(\rho\mathbf{u}_\alpha)), \tag{23}$$

where $p = \rho/3$ is the pressure, which gives a constant sound speed, $C_s = 1/\sqrt{3}$, and $\nu = (2\tau - 1)/6$ is the kinematic viscosity.

The resulting momentum equation is

$$\rho\left(\frac{\partial \mathbf{u}_\alpha}{\partial t} + \nabla_\beta \cdot \mathbf{u}_\alpha \mathbf{u}_\beta\right) = -\nabla_\alpha p + \nu \nabla_\beta \cdot (\nabla_\alpha \rho \mathbf{u}_\beta + \nabla_\beta \rho \mathbf{u}_\alpha), \tag{24}$$

which is exactly the same as the Navier-Stokes equations if the density variation $\delta\rho$ is small enough (Qian & Orszag 1993).

LBE: Approximation to the Continuum Boltzmann Equation

Although the LBE evolved from its Boolean counterpart, the LG automaton method, it has been shown recently by two groups independently (He & Luo 1997, Abe 1997) that the LBE can be obtained from the continuum Boltzmann equation for discrete velocities by using a small Mach number expansion. In these derivations, the starting point is the Boltzmann BGK equation (Bhatnagar et al 1954, Chu 1965, Xu & Prendergast 1994):

$$\frac{\partial g}{\partial t} + \boldsymbol{\xi} \cdot \nabla g = -\frac{1}{\varepsilon \tau}(g - g^{eq}), \tag{25}$$

where $g \equiv g(\mathbf{x}, \boldsymbol{\xi}, t)$ is the single-particle distribution function in continuum phase space $(\mathbf{x}, \boldsymbol{\xi})$, and g^{eq} is the Maxwell-Boltzmann equilibrium distribution function:

$$g^{eq} \equiv \frac{\rho}{(2\pi/3)^{D/2}} \exp\left[-\frac{3}{2}(\boldsymbol{\xi} - \mathbf{u})^2\right]. \tag{26}$$

Here D is the spatial dimension, and for simplicity, the particle velocity $\boldsymbol{\xi}$ and the fluid velocity $\mathbf{u}$ have been normalized by $\sqrt{3RT}$, giving a sound speed of $c_s = 1/\sqrt{3}$. T is the temperature. The macroscopic fluid variables are the velocity moments of the distribution function g:

$$\rho = \int g \, d\boldsymbol{\xi}, \qquad \rho\mathbf{u} = \int \boldsymbol{\xi} g \, d\boldsymbol{\xi}, \qquad \rho\varepsilon = \frac{1}{2}\int (\boldsymbol{\xi} - \mathbf{u})^2 g \, d\boldsymbol{\xi}, \tag{27}$$

where $\varepsilon = \frac{D}{2}T$ is the internal energy. Assuming that the fluid velocity in Equation 26 is a small parameter (compared with the sound speed), the equilibrium distribution g^{eq} up to $O(u^2)$ has the following form (Koelman 1991):

$$g^{eq} = \frac{\rho}{(2\pi/3)^{D/2}} \exp\left(-\frac{3}{2}\boldsymbol{\xi}^2\right)\left[1 + 3(\boldsymbol{\xi} \cdot \mathbf{u}) + \frac{9}{2}(\boldsymbol{\xi} \cdot \mathbf{u})^2 - \frac{3}{2}u^2\right]. \tag{28}$$

For discrete velocity models, only a small set of particle velocities $\mathbf{e}_i = \boldsymbol{\xi}_i$ $(i = 1, \ldots, M)$, and their distribution functions at these velocities, $g_i(\mathbf{x}, t) = g(\mathbf{x}, \mathbf{e}_i, t)$, are used; and the kinetic evolution in Equation 25 will only require the solution of g_i. The first two definitions in Equation 27 can be approximated using the discrete velocities in a Gaussian-type quadrature:

$$\rho(\mathbf{x}, t) = \sum_i W_i g_i(\mathbf{x}, t), \qquad \rho\mathbf{u}(\mathbf{x}, t) = \sum_i W_i \mathbf{e}_i g_i(\mathbf{x}, t). \tag{29}$$

This defines an effective distribution function $f_i(\mathbf{x}, t)$:

$$f_i(\mathbf{x}, t) = W_i g_i(\mathbf{x}, t), \tag{30}$$

which satisfies the simple conservation relations in Equation 3.

Given $\mathbf{e}_i$, W_i is constant, and f_i satisfies the same equation as g:

$$\frac{\partial f_i}{\partial t} + \mathbf{e}_i \cdot \nabla f_i = \frac{1}{\varepsilon \tau} \big(f_i^{eq} - f_i \big), \tag{31}$$

with $f_i^{eq} = w_i \rho [1 + 3(\mathbf{e}_i \cdot \mathbf{u}) + \frac{9}{2}(\mathbf{e}_i \cdot \mathbf{u})^2 - \frac{3}{2}u^2]$ and $w_i = W_i/(2\pi/3)^{D/2}$ $\exp(-\frac{3}{2}\mathbf{e}_i^2)$.

To obtain the weight w_i, He & Luo (1997) use a third-order Hermite formula to approximate the integrals in Equation 27. Abe (1997) assumes w_i has a simple truncated functional form based on $\mathbf{e}_i$. For the nine-velocity square lattice, both papers found that $w_0 = 4/9$, $w_i(i = 1, 3, 5, 7) = 1/9$ and $w_i(i = 2, 4, 6, 8) = 1/36$, which give the same equilibrium distribution function as the original lattice Boltzmann model in Equation 22.

If in Equation 31 the time derivative is replaced by a first order time difference, and the first order upwind discretization for the convective term $\mathbf{e}_i \cdot \nabla f_i$ is used and a downwind collision term $\Omega(\mathbf{x} - \mathbf{e}_i, t)$ for $\Omega(\mathbf{x}, t)$ is used (Cao et al 1997), then we obtain the finite difference equation for f_i:

$$f_i(\mathbf{x}, t + \Delta t) = f_i(\mathbf{x}, t) - \alpha \big[f_i(\mathbf{x}, t) - f_i(\mathbf{x} - \Delta x \mathbf{e}_i, t) \big]$$
$$- \frac{\beta}{\tau} \big[f_i(\mathbf{x} - \Delta x \mathbf{e}_i, t) - f_i^{eq}(\mathbf{x} - \Delta x \mathbf{e}_i, t) \big], \tag{32}$$

where $\alpha = \Delta t |\mathbf{e}_i|/\Delta x$, $\beta = \Delta t/\varepsilon$, and Δt and Δx are the time step and the grid step, respectively. Choosing $\alpha = 1$ and $\beta = 1$, Equation 32 becomes the standard LBE as shown in Equation 2.

From the discretization process, we note Equation 32 only has first order convergence in space and time to Equation 31. However, as shown by Sterling and Chen (1995), because Equation 32 has a Lagrangian nature in its spatial discretization, the discretization error has a special form which can be included in the viscous term, resulting in second-order accuracy both in space and time.

Boundary Conditions in the LBM

Wall boundary conditions in the LBM were originally taken from the LG method. For example, a particle distribution function bounce-back scheme (Wolfram 1986, Lavallée et al 1991) was used at walls to obtain no-slip velocity conditions. By the so-called bounce-back scheme, we mean that when a particle distribution streams to a wall node, the particle distribution scatters back to the node it came from. The easy implementation of this no-slip velocity condition by the bounce-back boundary scheme supports the idea that the

LBM is ideal for simulating fluid flows in complicated geometries, such as flow through porous media.

For a node near a boundary, some of its neighboring nodes lie outside the flow domain. Therefore the distribution functions at these no-slip nodes are not uniquely defined. The bounce-back scheme is a simple way to fix these unknown distributions on the wall node. On the other hand, it was found that the bounce-back condition is only first-order in numerical accuracy at the boundaries (Cornubert et al 1991, Ziegler 1993, Ginzbourg & Adler 1994). This degrades the LBM, because numerical accuracy of the LBM in Equation 2 for the interior mesh points is second-order. He et al (1997) confirmed this result by analyzing the slip velocity near the wall node for Poiseuille flow.

To improve the numerical accuracy of the LBM, other boundary treatments have been proposed. Skordos (1993) suggested including velocity gradients in the equilibrium distribution function at the wall nodes. Noble et al (1995) proposed using hydrodynamic boundary conditions on no-slip walls by enforcing a pressure constraint. Inamuro et al (1995) recognized that a slip velocity near wall nodes could be induced by the bounce-back scheme and proposed to use a counter slip velocity to cancel that effect. Maier et al (1996) modified the bounce-back condition to nullify net momentum tangent to the wall and to preserve momentum normal to the wall. Zou and He (1997) extended the bounce-back condition for the nonequilibrium portion of the distribution. Ziegler (1993) noticed that if the boundary was shifted into fluid by one half mesh unit, i.e. placing the nonslip condition between nodes, then the bounce-back scheme will give second-order accuracy. Simulations demonstrated that these heuristic models yield good results for fluid flows around simple wall boundaries. The above boundary treatments were also analyzed by Zou et al (1995) and He et al (1997) by solving the lattice BGK equation (Equation 2). It appears, however, that the extension of these simple assumptions to arbitrary boundary conditions is difficult. Chen et al (1996) viewed the LBM as a special finite difference scheme of the kinetic equation (Equation 31). They adopted staggered mesh discretization from traditional finite difference methods and proposed using a second-order extrapolation scheme of distributions in the flow to obtain the unknown particle distribution functions. Their extrapolation scheme is simple and can be extended to include velocity, temperature, and pressure (Maier et al 1996, Zou & He 1997) boundary conditions and their derivatives. In this treatment, boundary conditions can be assigned to grid nodes or to any locations in space for little computational effort. Numerical simulations including time-dependent Couette flow, a lid-driven square-cavity flow, and flow over a column of cylinders were carried out, showing good agreement with analytical solutions and finite difference solutions.

Numerical Efficiency, Stability, and Nonuniform Grid

The discrete velocity equation (Equation 31) is a hyperbolic equation that approximates the Navier-Stokes equation in the nearly-incompressible limit (Majda 1984). The numerical accuracy depends on Mach number (Reider & Sterling 1995). The advective velocity $\mathbf{e}_i$ in Equation 31 is a constant vector, in contrast to the spatial dependent velocity in compressible hydrodynamic equations, which prevents the LBM from solving nonlinear Riemann problems. From a numerical analysis point of view, the LBM, like other kinetic equations, is a relaxation method (Cao et al 1997) for the macroscopic equations, which has much in common with the explicit "penalty" or "pseudocompressibility method" (Sterling & Chen 1996). This view was used by Ancona (1994) to generalize the LBM to include fully Lagrangian methods for the solution of partial differential equations. The advective velocity $\mathbf{e}_i$ in Equation 31 is constant in contrast to the spatial dependent velocity in compressible hydrodynamic equations. The kinetic-relaxation method for solving a hyperbolic conservation system was proposed by Jin and Xin (1995). This approach uses the relaxation approach to model the nonlinear flux terms in the macroscopic equations and thus it does not require nonlinear Riemann solvers either. Using this relaxation method, Jin and Katsoulakis (1997) calculated curvature-dependent front propagation. In principle, the LBM and the kinetic-relaxation method are very much alike. The kinetic-relaxation was developed mainly for shock capture in Euler systems, whereas the LBM is more focused on viscous complex flows in the nearly-incompressible limit. Nadiga and Pullin (1994) proposed a simulation scheme for kinetic discrete-velocity gases based on local thermodynamic equilibrium. Their method seems more general and able to obtain high order numerical accuracy. Their finite volume technique was further developed (Nadiga 1995) to solve the compressible Euler equation by allowing the discrete velocities to adapt to the local hydrodynamic state. Elton et al (1995) studied issues of convergence, consistency, stability, and numerical efficiency for lattice Boltzmann models for viscous Burgers' equation and advection-diffusion system.

The numerical efficiency of the LBM was studied by several authors. Succi et al (1991) noted that the number N_{fpo} of floating point calculations for the LBM would be $\sim r N^D$, while $N_{fpo} \sim (25 \log_2 N) N^D$ for the pseudospectral method, where N is the number of lattice points along each direction in D dimensions. r is 150 for the two-dimensional LBM using the full matrix M_{ij} in Equation 10 and 40 for the LBGK model. For 3-D low Reynolds number simulations, an LBM performance of 2.5 times faster than the pseudo-spectral method was reported (Chen et al 1992). The scalability of the LBM was studied by Noble et al (1996). They found a better-than-linear scalability for the LBM

when the number of processors increases while simultaneously increasing size of the computational domain. For a 2-D problem with 2176^2 lattice points, they achieved an overall 13.9 gigaflops using 512 processors of CM-5 machines.

In the continuum Boltzmann equation, the equilibrium distribution function given by Equation 26 corresponds to the maximum entropy state. Thus, any initial state will evolve towards a state of higher entropy. This result is known as Boltzmann's H-theorem, which ensures an increase of entropy and ensures stability. An H-theorem has been derived also for the LG method (Frisch et al 1987). In the LBM, however, only a small number of discrete velocities is used and usually the equilibrium distribution is truncated to $O(u^2)$ (see Equation 21). Consequently, one cannot simultaneously guarantee an H-theorem and allow the correct form of the macroscopic equations. Therefore, the LBM, although of a kinetic nature, is subject to numerical instability. Furthermore, we know also that the traditional LBM equation (Equation 2) is a finite-difference solution of the discrete-velocity Boltzmann equation in Equation 31 and the discretization in Equation 32 with $\alpha = 1$ marginally satisfies the Courant-Friedrichs-Lewy condition. A von Neumann linearized stability analysis of the LBM was carried out by Sterling & Chen (1996). In this analysis, they expanded f_i as $f_i(\mathbf{x}, t) = f_i^{(0)} + f_i'(\mathbf{x}, t)$, where the global equilibrium populations $f_i^{(0)}$ were assumed to be constants that depend only on a constant mean density and constant velocity. Taylor-expanding Equation 2, they arrived at the following linearized equation:

$$f_i'(\mathbf{x} + \mathbf{e}_i \Delta t, t + \Delta t) = J_{ij} f_j'(x, t), \tag{33}$$

where J_{ij} is the Jacobian matrix corresponding to the coefficient of the linear term in Equation 2 and does not depend on location or time. Spatial dependence of the stability analysis was carried out by taking the Fourier transformation of Equation 33 and solving the eigenvalue problem for $\mathrm{diag}[\exp(-i\mathbf{k} \cdot \mathbf{e}_i \Delta t)]J_{ij}$. For $\mathbf{k} = 0$, they found the linear stability condition: $\tau \leq 1/2$ which is consistent with the positivity of viscosity. Detailed stability analysis were carried out for the hexagonal 2-D LBM model (Chen et al 1992), the square 2-D LBM model and the 3-D 15-velocity model (Qian et al 1992). They concluded that a stable LBM requires that the mean flow velocity be below a maximum velocity that is a function of several parameters, including the sound speed C_s, the relaxation time τ, and the wave number. The numerical stability can also be improved if one starts from the continuum kinetic equation (Equation 31) (Ancona 1994, McNamara et al 1995, Cao et al 1997) using different finite difference discretizations.

Until recently, one of the limitations to the numerical efficiency in the LBM, as compared with other CFD methods, is that the discretization of Equation 31 was constrained on a special class of uniform and regular lattices. To increase

numerical efficiency and accuracy, nonuniform grid methods have been developed. Koelman (1991) suggested including spatial nonuniformity in the lattice structure. Nannelli & Succi (1992) and Amati et al (1997) developed the finite volume LBM (FVLBM) based on Equation 31. They defined a nonuniform coarse lattice whose cell typically contained several original lattice units. The evolution equation for the mean value $F_i \equiv V_C^{-1} \int_C f_i d^3x$ in the Cell C requires the evaluation of the flux across the boundaries of C, where V_C is the volume. A piece-wise constant or a piece-wise linear interpolation was used to approximate the flux. This FVLBM has been used to study two-dimensional flow past a bluff body (Succi & Nannelli 1994) and three-dimensional turbulent channel flow (Amati et al 1997). The results of the 3-D channel flow simulation reveal that the FVLBM is about one order of magnitude faster than the traditional nonuniform CFD methods. On the other hand, while most simulation results agree well with other traditional methods, the comparison of simulation results is correspondingly less satisfactory, owing partially to the low-order interpolation schemes. Cao et al (1997) developed a nonuniform finite difference LBM for Equation 31 and simulated annular flows in polar coordinates. He et al (1996) adhered to the LBM equation (Equation 2) and developed a time-dependent interpolation scheme that increases grid density in high-shear regions. They successfully simulated flows in the 2-D symmetric channel with sudden expansion and flow around a circular cylinder (He & Doolen 1997).

LATTICE BOLTZMANN SIMULATION OF FLUID FLOWS

Flows with Simple Boundaries

DRIVEN CAVITY FLOWS   For two-dimensional cavity flows, there are many papers using traditional schemes, including finite-difference (Schreiber & Keller 1983, E & Liu 1996) and multigrid (Vanka 1986). The fundamental characteristics of the 2-D cavity flow are the emergence of a large primary vortex in the center and two secondary vortices in the lower corners. The values of the stream function and the locations of the centers of these vortices as a function of Reynolds numbers have been well studied. The lattice Boltzmann simulation of the 2-D driven cavity by Hou et al (1995) covered a wide range of Reynolds numbers from 10 to 10,000 using a 256^2 lattice. They carefully compared simulation results of the stream function and the locations of the vortex centers with previous numerical simulations and demonstrated that the differences of the values of the stream function and the locations of the vortices between the LBM and other methods were less than 1%. This difference is

within the numerical uncertainty of the solutions using other numerical methods. The spatial distributions of the velocity, pressure and vorticity fields were also carefully studied. An error analysis of the compressibility effect from the model was carried out. Two-dimensional cavity flow was also studied by Miller (1995). Instead of using a uniform velocity on the top of the cavity, in Miller's work a shear-flow condition with certain velocity distribution was given which allowed an analytical solution of the velocity for the whole cavity. Excellent agreement between the LBM simulations and the analytical solutions for the velocity and pressure fields was found. The effects of the variation of the cavity aspect ratio on vortex dynamics were also studied.

Hou (1995) simulated three-dimensional cubic cavity flow using the three-dimensional 15-velocity LBM (Qian et al 1992, Chen et al 1992). 128^3 lattice points were used with Re = 3,200. Flows at this Reynolds number had been extensively studied earlier, including the finite-difference simulation and the experimental work by Prasad & Koseff (1989). Flow structures, including the velocity and vorticity fields in different planes were analyzed using the LBM simulation. They compared well with previous numerical studies. The correlation of the Taylor-Görtler-like vortices in the yz- and xz-planes was reported for the first time. Figure 1 displays the mean velocity profiles from 3-D LBM, 2-D LBM simulations, and experimental work (Prasad & Koseff 1989) in the symmetry plane along the vertical and the horizontal centerlines (*left*), and the root-mean-square (*rms*) velocity profiles (*right*). The agreement
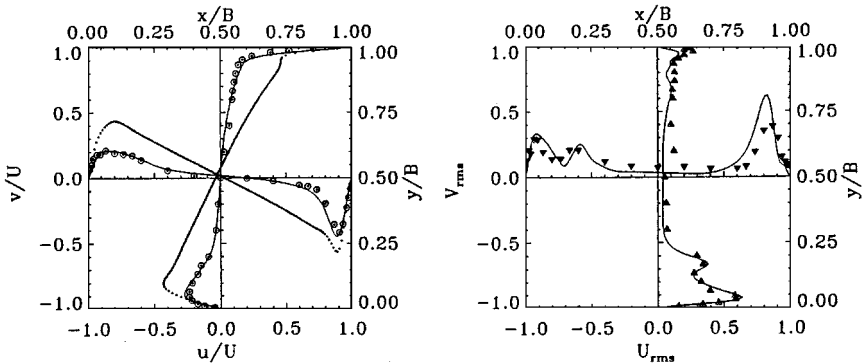

Figure 1   Mean velocity profiles (*left*), $\frac{\bar{u}}{U}$ and $\frac{\bar{v}}{U}$, in the symmetry plane along the vertical and the horizontal centerlines. *Solid line* is for the 3-D LBE simulation, *dotted line* is a 2-D simulation (Hou 1995), and *circles* represent experimental results (Prasad & Koseff 1989). *rms* velocities (*right*), U_{rms} and V_{rms}, in the symmetry plane along vertical and horizontal centerlines. *Solid line* is the LBE simulation, *upward triangles* and *downward triangles* are experimental results (Prasad & Koseff 1989).

between the 3-D LBM results and experimental results shows that the LBM is capable of simulating complex 3-D unsteady flows.

FLOW OVER A BACKWARD-FACING STEP   The two-dimensional symmetric sudden expansion channel flow was studied by Luo (1997) using the LBM. The main interest in Luo's research was to study the symmetry-breaking bifurcation of the flow when Reynolds number increases. In this simulation, an asymmetric initial perturbation was introduced and two different expansion boundaries, square and sinusoidal, were used. This simulation reproduced the symmetric-breaking bifurcation for the flow observed previously, and obtained the critical Reynolds number of 46.19. This critical Reynolds number was compared with earlier simulation and experimental results of 40.45 and 47.3, respectively. Qian et al (1996) used the flow over a backward-facing step as a benchmark for validating the LBM. They studied the recirculation length as a function of Reynolds number and the channel expansion ratio. The results from the LBM compared well with previous results using finite-difference methods, spectral-element methods, and experiments. The appearance of the second vortex and the transition leading to turbulence were also studied.

FLOW AROUND A CIRCULAR CYLINDER   The flow around a two-dimensional circular cylinder was simulated using the LBM by several groups of people. The flow around an octagonal cylinder was also studied (Noble et al 1996). Higuera & Succi (1989) studied flow patterns for Reynolds number up to 80. At $\text{Re} = 52.8$, they found that the flow became periodic after a long initial transient. For $\text{Re} = 77.8$, a periodic shedding flow emerged. They compared Strouhal number, flow-separation angle, and lift and drag coefficients with previous experimental and simulation results, showing reasonable agreement. Pressure distributions around the surface of the cylinder as a function of Reynolds number were carefully studied by Wagner (1994). He concluded that the difference between his Strouhal numbers and those from other simulations was less than 3.5%. Considering the compressible nature of the LBM scheme, this result is significant. It demonstrates that in the nearly incompressible limit, the LBM simulates the pressure distribution for incompressible fluids well (Martinez et al 1994). The above two simulations were based on uniform lattices, which poorly approximate circular geometry. The no-slip boundary was enforced at the boundary mesh point which is jagged and not necessary on the cylinder. He & Doolen (1997) revisited the problem of two-dimensional flow around a circular cylinder based on the interpolation-supplement LBM (He et al 1996). In this simulation, the underlying lattice was square, but a spatial interpolation was used. A polar coordinate was constructed and the simulation domain consisted of a circular region. The no-slip wall boundary condition was exactly enforced

on the cylinder boundary. It is clear that the computational accuracy in this simulation is better than previous LBM simulations. The streaklines showed vortex shedding quite similar to experimental observation. The LBM calculated Strouhal numbers. Lift and drag coefficients for flows at different Reynolds numbers compared well with previous simulations using other schemes. The error was within experimental uncertainty and is the same as errors among other schemes.

Flows in Complex Geometries

An attractive feature of the LBM is that the no-slip bounce-back LBM boundary condition costs little in computational time. This makes the LBM very useful for simulating flows in complicated geometries, such as flow through porous media, where wall boundaries are extremely complicated and an efficient scheme for handing wall-fluid interaction is essential.

The fundamental problem in the simulation of fluid flows through porous media is to understand and model the macroscopic transport from microscopic fluid dynamics. A starting point for this problem is Darcy's law, which assumes a linear relation between the pressure gradient, $\Delta P/L$, and the volume flow rate per unit area q: $q = -K/(\rho_0 \nu)\Delta P/L$. Here K is the permeability. Previous numerical simulations, including finite-difference schemes (Schwarz et al 1994) and networking models (Koplik & Lasseter), were either limited to simple physics, small geometry size, or both. Lattice gas automata were also used for simulating porous flows and verifying Darcy's law in simple and complicated geometries (Rothman 1988). Succi et al (1989) utilized the LBM to measure the permeability in a 3-D random media. Darcy's law was confirmed. Cancelliere et al (1990) studied the permeability K as a function of solid fraction η in a system of randomly positioned spheres of equal radii. The simulation covered a wide range of η ($0.02 \leq \eta \leq 0.98$). The values of K from the LBM compared well with the Brinkman approximation: $K = K_0[1 + 3/4\eta(1 - \sqrt{8/\eta - 3})]$ for $\eta < 0.2$, and agreed well with the semiempirical Kozeny-Carman equation: $K = (1 - \eta)^3/(6s^2)$. Here K_0 is the effective permeability for a single sphere and s is the specific surface area for the system. Later, Heijs & Lowe (1995) confirmed this result independently. In addition, they studied the validity of the Kozeny-Carman equation for soil samples where flow occurs only through some specific continuous connected pore and flows occurring at smaller scales are negligible. For this condition, the Kozeny-Carman equation provided a much less successful estimate of the permeability. Flows through sandstones measured using X-ray microtomography were simulated by Buckles et al (1994), Soll et al (1994), and Ferréol & Rothman (1995). They found that the permeability for these sandstones, although showing large variation in space and flow directions, in general agreed well with experimental measurements

within experimental uncertainty. Ferréol & Rothman (1995) also studied the effect of grid resolution on permeability. They found that the permeability strongly depends on the viscosity when the minimum channel in the pores is several grid points wide.

Spaid & Phelan (1997) investigated the injection process in resin transfer molding. For this heterogeneous porous media simulation, they used the LBM simulation of full Navier-Stokes flows to model a flow around a circular cylinder. Inside the cylinder, the velocity is governed by the Brinkman equation ($\nu\nabla^2\mathbf{u} - \beta u = \nabla P/\rho$, where β is a model parameter). Excellent agreement between the LBM simulation and lubrication theory for cell permeabilities was reported.

Simulation of Fluid Turbulence

DIRECT NUMERICAL SIMULATION   A major difference between the LBM and the LG method is that the LBM can be used for smaller viscosities. Consequently the LBM can be used for direct numerical simulation (DNS) of high Reynolds number fluid flows. To validate the LBM for simulating turbulent flows, Martinez et al (1994) studied decaying turbulence of a shear layer using both the pseudospectral method and the LBM. The initial shear layer consisted of uniform velocity reversing sign in a very narrow region. The initial Reynolds number was 10,000. The simulation used a 512^2 mesh and ran for 80 large-eddy turnover times. Martinez et al carefully compared the spatial distribution, time evolution of the stream functions, and the vorticity fields. Energy spectra as a function of time, small scale quantities, including enstrophy, palinstrophy, and 4th-order enstrophy as a function of time were also studied. The correlation between vorticity and stream function was calculated and compared with theoretical predictions. They concluded that the LBE method provided a solution that was "accurate" in the sense that time histories of global quantities, wavenumber spectra, and vorticity contour plots were very similar to those obtained from the spectral method. In particular, they reproduced details of the wavenumber spectra at high wavenumbers as well as the detailed structure of vortex distributions. Their conclusions are significant for simulations of turbulence in which small-scale dynamics are important. In that paper they found discrepancies in the spatial locations of vortical structures at very late stages.

Figure 2 (*top left*) compares the energy spectra from a pseudospectral method (*dotted line*) and the LBM (*solid line*) for $t = 5$, and displays the time evolution of the enstrophy function (*bottom left*). Figure 2 also depicts contour plots of the vorticity function at the same time step (*right*). The agreement of these two methods is excellent. Two-dimensional forced isotropic turbulence was simulated by Benzi & Succi (1990) to study the enstrophy cascade range. Two-dimensional forced turbulence was also simulated by Qian et al (1995) to study
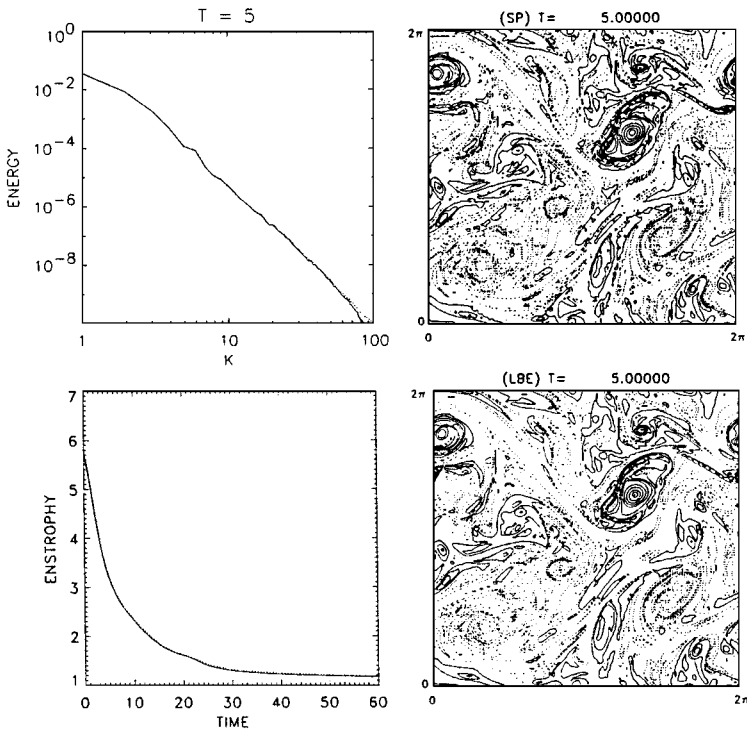
Figure 2   Velocity energy spectra versus wavenumber, k (*top left*). The enstrophy of the system, $\langle \omega^2 \rangle$ (*bottom left*), as a function of time. *Right*, a comparison of the vorticity distributions from a pseudospectral method and the LBM (Martinez et al 1994).

the energy inverse cascade range. They reproduced the $k^{-5/3}$ inertial range scaling, in good agreement with theoretical predictions (Kraichnan 1967).

Chen et al (1992) made a similar validation of LBM by comparing results of three-dimensional isotropic turbulence using the LBM and the pseudospectral method. In that work, they simulated three-dimensional Beltrami flows, the decaying Taylor-Green vortex, and decaying three-dimensional turbulence. The agreement between the two methods for spatial and time distributions of velocities and vortices was good. This assessment was echoed by Treviño & Higuera (1994), who studied the nonlinear stability of Kolmogorov flows using the pseudospectral method and the LBM at various Reynolds numbers.

The LBM is a useful direct numerical simulation (DNS) tool for simulating nonhomogeneous turbulent flows. To validate the generalized extended self-similarity for anisotropic flows where the simple extended self-similarity is not

valid, Benzi et al (1996) used the LBM to simulate three-dimensional shear flow where a sinusoidal force in the x direction varying along the z direction was applied. This simulation generated useful velocity and vorticity information, and the scaling exponents of the velocity increment and their dependence on the shear rate were studied. Based on their analysis of this flow, they concluded that the generalized extended self-similarity was valid for anisotropic flows. Succi et al (1991) studied the bifurcation of a two-dimensional Poiseuille flow and obtained the amplitude of the primary and secondary bifurcated models as a function of the Reynolds number. Eggels (1996) utilized the LBM on the FCHC lattice (d'Humières et al 1986) as a DNS method for simulating three-dimensional channel flows with $Re_* = 180$ (based on the friction velocity). Their simulation results, including mean stream-wise velocity profiles and rms velocities as functions of the distance from the wall, were compared with those reported by Kim et al (1987), showing good agreement.

LBM MODELS FOR TURBULENT FLOWS   As in other numerical methods for solving the Navier-Stokes equations, a subgrid-scale (SGS) model is required in the LBM to simulate flows at very high Reynolds numbers. Direct numerical simulation is impractical due to the time and memory constraints required to resolve the smallest scales (Orszag & Yakhot 1986). Hou et al (1996) directly applied the subgrid idea in the Smagorinsky model to the LBM by filtering the particle distribution function and its equation in Equation 2 using a standard box filter. To account for the nonlinear term in the equilibrium distribution (Equation 22), Hou et al (1996) replaced the relaxation time τ in Equation 13 by $(3\nu_0 + C_s^2 \Delta^2 |\overline{S}|^2) + 1/2$, where $\nu_0 = (2\tau - 1)/6$ is the kinetic viscosity, Δ is the filter width, $|\overline{S}|$ is the amplitude of the filtered large-scale strain-rate tensor, and C_s is the Smagorinsky constant. This simple Smagorinsky-type LBM subgrid model was used to simulate flows in a two-dimensional cavity at Reynolds numbers up to 10^6 using a 256^2 mesh (Hou et al 1996). Three-dimensional turbulent pipe flow was simulated by Somers (1993) using the LBM SGS model at a Reynolds number of 50,000 for mesh sizes up to 80^3. Friction as a function of Reynolds number compared reasonably well with the Blasius power law for turbulent flows. Succi et al (1995) suggested using the relaxation idea in the LBM to solve the turbulent $K - \epsilon$ equations. Hayot & Wagner (1996) used a dependent relaxation $\tau(t)$ in the lattice BGK equation (Equation 13), which leads to an effective turbulent viscosity. Eggels (1996) and Eggels & Somers (1995) included the turbulent stress tensor σ_t directly into the equilibrium distribution, f_i^{eq} in Equation 22, by adding an extra term: $f_i^{\sigma} = \rho[\mathbf{e}_{i\alpha}\mathbf{e}_{i\beta}\sigma_{t\alpha\beta} - \frac{M}{D}\mathrm{tr}(\sigma_t)]$. Using this model, Eggels (1996) carried out a large-eddy simulation of the turbulent flow in a baffled stirred tank reactor. The impact of a mechanical impeller was modeled via a spatial and temporal

dependent force on the momentum equation. It was reported that the subgrid LBE turbulent model coupled with the impeller model produced satisfactory results. Both mean flow and turbulent intensities compared well with experimental data. This simulation demonstrated the potential of the LBM SGS model as a useful tool for investigating turbulent flows in industrial applications of practical importance.

LBM SIMULATIONS OF MULTIPHASE AND MULTICOMPONENT FLOWS

The numerical simulation of multiphase and multicomponent fluid flows is an interesting and challenging problem because of difficulties in modeling interface dynamics and the importance of related engineering applications, including flow through porous media, boiling dynamics, and dendrite formation. Traditional numerical schemes have been successfully used for simple interfacial boundaries (Glimm et al 1981, Brackbill et al 1992, Chang et al 1996). The LBM provides an alternative for simulating complicated multiphase and multicomponent fluid flows, in particular for three-dimensional flows.

Method of Gunstensen et al

Gunstensen et al (1991) were the first to develop the multicomponent LBM method. It was based on the two-component LG model proposed by Rothman & Keller (1988). Later, Grunau et al (1993) extended this model to allow variations of density and viscosity. In these models, red and blue particle distribution functions $f_i^{(r)}(\mathbf{x}, t)$ and $f_i^{(b)}(\mathbf{x}, t)$ were introduced to represent two different fluids. The total particle distribution function (or the color-blind particle distribution function) is defined as: $f_i = f_i^{(r)} + f_i^{(b)}$. The LBM equation is written for each phase:

$$f_i^k(\mathbf{x} + \mathbf{e}_i, t + 1) = f_i^k(\mathbf{x}, t) + \Omega_i^k(\mathbf{x}, t),\tag{34}$$

were k denotes either the red or blue fluid, and

$$\Omega_i^k = \left(\Omega_i^k\right)^1 + \left(\Omega_i^k\right)^2\tag{35}$$

is the collision operator. The first term in the collision operator, $(\Omega_i^k)^1$, represents the process of relaxation to the local equilibrium similar to the LBGK model in Equation 13:

$$\left(\Omega_i^k\right)^1 = \frac{-1}{\tau_k}\left(f_i^k - f_i^{k(eq)}\right).\tag{36}$$

Here, $f_i^{k(eq)}$ is the local equilibrium distribution depending on the local macroscopic variables $\rho^{(k)}$ and $\mathbf{u}^{(k)}$. τ_k is the characteristic relaxation time for species

k. The viscosity of each fluid can be selected by choosing the desired τ_k. Conservation of mass for each phase and total momentum conservation are enforced at each node during the collision process:

$$\rho_r = \sum_i f_i^r = \sum_i f_i^{r(eq)}, \qquad \rho_b = \sum_i f_i^b = \sum_i f_i^{b(eq)},$$

$$\rho\mathbf{u} = \sum_{i,k} f_i^k \mathbf{e}_i = \sum_{i,k} f_i^{k(eq)} \mathbf{e}_i, \tag{37}$$

where $\rho = \rho_r + \rho_b$ is the total density and $\rho\mathbf{u}$ is the local total momentum. The form of $f_i^{k(eq)}$ can be chosen to be similar to Equation 22.

The additional collision operator $(\Omega^k)^2$ contributes to the dynamics in the interfaces and generates a surface tension:

$$\left(\Omega_i^k\right)^2 = \frac{A_k}{2}|\mathbf{F}|\left((\mathbf{e}_i \cdot \mathbf{F})^2/|\mathbf{F}|^2 - 1/2\right), \tag{38}$$

where $\mathbf{F}$ is the local color gradient, defined as:

$$\mathbf{F}(\mathbf{x}) = \sum_i \mathbf{e}_i(\rho_r(\mathbf{x} + \mathbf{e}_i) - \rho_b(\mathbf{x} + \mathbf{e}_i)). \tag{39}$$

Note that in a single-phase region of the incompressible fluid model, $\mathbf{F}$ vanishes. Therefore, the second term of the collision operator $(\Omega_i^k)^2$ only contributes to interfaces and mixing regions. The parameter A_k is a free parameter, which determines the surface tension. The additional collision term in Equation 38 does not cause the phase segregation. To maintain interfaces or to separate the different phases, the LBM by Gunstensen et al follows the LG method of Rothman & Keller (1988) to force the local color momentum, $\mathbf{j} = \sum_i(f_i^r - f_i^b)\mathbf{e}_i$, to align with the direction of the local color gradient after collision. In other words, the colored distribution functions at interfaces were redistributed to maximize $-\mathbf{j} \cdot \mathbf{F}$. Intuitively, this step will force colored fluids to move toward fluids with the same colors.

The multicomponent LBM by Gunstensen et al (1991) has two drawbacks. First, the procedure of redistribution of the colored density at each node requires time-consuming calculations of local maxima. Second, the perturbation step with the redistribution of colored distribution functions causes an anisotropic surface tension that induces unphysical vortices near interfaces. D'ortona et al (1994) modified the model of Gunstensen et al. In their model, the recoloring step is replaced by an evolution equation for f_i^k that increases computational efficiency.

Method of Shan & Chen

Shan & Chen (1993) and Shan & Doolen (1995) used microscopic interactions to modify the surface-tension–related collision operator for which the surface

interface can be maintained automatically. In these models, $(\Omega_i^k)^2$ in Equation 38 was replaced by the following formula:

$$\left(\Omega_i^k\right)^2 = \mathbf{e}_i \cdot \mathbf{F}^k. \tag{40}$$

Here $\mathbf{F}^k$ is an effective force on the kth phase owing to a pairwise interaction between the different phases:

$$\mathbf{F^k}(\mathbf{x}) = -\sum_{k'} \sum_i V_{kk'}(\mathbf{x}, \mathbf{x} + \mathbf{e}_i)\mathbf{e}_i. \tag{41}$$

Here $V_{kk'}$ is an interaction pseudopotential between different phases (or components):

$$V_{kk'}(\mathbf{x}, \mathbf{x}') = G_{kk'}(\mathbf{x}, \mathbf{x}')\psi^k(\mathbf{x})\psi^{k'}(\mathbf{x}'). \tag{42}$$

$G_{kk'}(\mathbf{x})$ is the strength of the interaction; and $\psi^k(\mathbf{x})$ is a function of density for the k phase at $\mathbf{x}$ which has taken the following empirical form: $\psi = \rho_0[1 - \exp(-\rho/\rho_0)]$, where ρ_0 is a constant free parameter. It was shown that this form of the effective density ψ gives a non-ideal equation of state, which separates phases or two component fluids. Qian et al (1995) have recently demonstrated that other pseudopotential forms, including fractional potential and a van der Waals potential, will produce similar results.

It should be noted that the collision operator $(\Omega_i^k)^2$ in the Shan-Chen model does not satisfy local momentum conservation. This treatment is physically plausible because the distant pairwise interactions between phases change the point-wise local momenta at the positions involved in the interactions. This feature differs from the model of Gunstensen et al where the total local momentum is conserved (see the third operation in Equation 37). It is arguable that this spurious conservation might be one reason why the model exhibits unphysical features near interfaces.

For simplicity, only the nearest-neighbor interactions were involved in the Shan-Chen model, in which $G_{kk'}(\mathbf{x}, \mathbf{x}')$ is constant when $\mathbf{x} - \mathbf{x}' = \mathbf{e}_i$, and zero otherwise. $G_{kk'}$ acts like a temperature; when G is smaller than the critical value G_c (depending on the lattice structure and initial density), the fluids separate. Theoretical calculations indicate (Shan & Chen 1994) that the surface tension $\sigma \sim MG/[2D(D + 1)]$, which was also verified by numerical simulation.

In the Shan-Chen model, the separation of fluid phases or components is automatic (Chen 1993). This is an important improvement in numerical efficiency compared with the original LBM multiphase models. The Shan-Chen model also improves the isotropy of the surface tension.

Free Energy Approach

The above multiphase and multicomponent lattice Boltzmann models are based on phenomenological models of interface dynamics and are probably most

suitable for isothermal multicomponent flows. One important improvement in models using the free-energy approach (Swift et al 1995, 1996) is that the equilibrium distribution can be defined consistently based on thermodynamics. Consequently, the conservation of the total energy, including the surface energy, kinetic energy, and internal energy can be properly satisfied (Nadiga & Zaleski 1996).

The van der Waals formulation of quasilocal thermodynamics for a two-component fluid in thermodynamic equilibrium at a fixed temperature has the following free-energy functional:

$$\Psi(\mathbf{r}) = \int d\mathbf{r}[\psi(T, \rho) + W(\nabla\rho)]. \tag{43}$$

The first term in the integral is the bulk free-energy density, which depends on the equation of state. The second term is the free-energy contribution from density gradients and is related to the surface tension. For simple multiphase fluid flows, $W = \frac{\kappa}{2}(\nabla\rho)^2$, where κ is related to the surface tension. The full pressure tensor in a nonuniform fluid has the following form:

$$P_{\alpha\beta} = p\delta_{\alpha\beta} + \kappa\frac{\partial\rho}{\partial x_\alpha}\frac{\partial\rho}{\partial x_\beta}. \tag{44}$$

The pressure is obtained from the free energy: $p(\mathbf{r}) = \rho\frac{\delta\Psi}{\delta\rho} - \Psi(\mathbf{r}) = p_0 - \kappa\rho\nabla^2\rho - \frac{\kappa}{2}(\nabla\rho)^2$, where $p_0 = \rho\psi'(\rho) - \psi(\rho)$ is the equation of state. For a van der Waals equation of state, $\psi = \rho T\ln\rho/(1 - \rho b) - a\rho^2$, where a and b are free parameters.

To incorporate the above formulation into the lattice Boltzmann equation, Swift et al (1995) added a term to the original equilibrium distribution in Equation 21: $f_i^{eq'} = f_i^{eq} + G_{\alpha\beta}\mathbf{e}_{i\alpha}\mathbf{e}_{i\beta}$. They vary the coefficients in f_i^{eq} (see Equation 21) and $G_{\alpha\beta}$ to guarantee the conservation of mass and momentum and to obtain the following stress tensor condition: $\sum_i f_i^{eq'}\mathbf{e}_{i\alpha}\mathbf{e}_{i\beta} = P_{\alpha\beta} + \rho u_\alpha u_\beta$.

Numerical Verification and Applications

Two fundamental numerical tests associated with interfacial phenomena have been carried out using the multiphase and multicomponent lattice Boltzmann models. In the first test, the lattice Boltzmann models were used to verify Laplace's formula by measuring the pressure difference between the inside and the outside of a droplet: $P_{inner} - P_{outer} = \frac{\sigma}{R}$, where P_{inner} and P_{outer} denote the pressures inside and outside of the droplet, respectively. R is the radius of the droplet and σ is the surface tension. The simulated value of σ has been compared with theoretical predictions, and good agreement was reported (Gunstensen et al 1991, Shan and Chen 1993, Swift et al 1995). Alternatively,

the surface tension can also be measured using the mechanical definition

$$\sigma = \int_{-\infty}^{\infty} (P_N - P_T)dz, \tag{45}$$

where P_N and P_T are the normal and the tangential pressure along a flat inter-
face, respectively, and the integration is evaluated in a direction perpendicular
to the interface. It is shown from LBM simulations (Gunstensen et al 1991,
Grunau et al 1993, Swift et al 1995) that the surface tension obtained from the
mechanical definition agrees with the Laplace formula definition.

In the second test of LBM interfacial models, the oscillation of a capillary
wave was simulated (Gunstensen et al 1991, Shan & Chen 1994, Swift et al
1995). A sine wave displacement of a given wave vector was imposed on an
interface that had reached equilibrium. The resulting dispersion relation was
measured and compared with the theoretical prediction (Laudau & Lifshitz
1959): $\omega^2 = \sigma/\rho k^3$. Good agreement was observed, validating the LBM
surface tension models.

Because the lattice Boltzmann multiphase and multicomponent models do
not track interfaces, it is easy to simulate fluid flows with very complicated
interfaces, such as the domain growth in the spinodal decomposition process for
binary fluids (Alexander et al 1993a, Rybka et al 1995). In these simulations,
hydrodynamics plays an important role and multiphase or multicomponent
fluids evolved from an initial mixed state owing to surface tension, viscosity,
and inertial force.

A convenient way to characterize the growth kinetics is to use the correlation
function of the order parameter, $G(r, t) \equiv \langle \phi(r)\phi(0) \rangle$, where ϕ is the order
parameter, defined as $(\rho_r - \rho_b)/(\rho_r + \rho_b)$. The Fourier transform of $G(r, t)$
is then the structure function S(k,t). As time evolves, the structure function
becomes more sharply peaked, and its maximum value moves toward small
k. In a wide variety of phase segregating systems, S(k,t) has a simple form at
late times: $S(k, t) = R^D(t)F(x)$. Here $R(t)$ is the average domain size, D
is the dimension, and $F(x)$ is a universal function depending on $x = kR(t)$.
Numerical calculations of $R(t)$ and $F(x)$ have been carried out using the LBM
(Alexander et al 1993a). It was found that $R(t)$ scales $\sim t^{2/3}$ in two dimen-
sions and $\sim t$ in three dimensions for two-component fluids. This agrees with
theoretical predictions. $F(x)$ was found to agree well with Porod's law for
large x, $\sim x^{D+1}$, but small scales showed strong dependence of flow properties,
which was later confirmed by Wu et al (1995) using the Langevin equation.
Osborn et al (1995) studied similar scaling problems for liquid-gas two-phase
domain growth. They found that $R(t) \sim t^{1/2}$ and $\sim t^{2/3}$ at high and low vis-
cosities, respectively. A similar crossover for two-component fluids from $t^{1/3}$
to $t^{2/3}$ was also reported as time increased. The hydrodynamic effects on the

spinodal decomposition for three and four components in two and three dimensions in critical and off-critical quenching were also studied by Chen & Lookman (1995). Cieplak (1995) carried out a study of two-dimensional rupture dynamics under initial perturbation and compared results with molecular dynamics simulations. The coalescence process was also studied for a droplet in a background fluid falling in a gravitational field to the bottom of a container in which the bottom is a "bare" wall, a shallow liquid with the same kind as the droplet, or a deeper liquid. Interesting interfacial structures were observed.

In Figure 3 we show condensation and subsequent coalescence of liquid drops in supersaturated vapor at two different times. The LBE model with interparticle interaction (Shan & Chen) was used in this simulation on a 128^3 lattice. The fluid obeys the equation of state: $p = \frac{1}{3}\rho + \frac{3}{2}G(1 - e^{-\rho})^2$. G (chosen to be -0.55) is a parameter that gives the relative strength of the interaction. This equation of state gives a non-monotonic isotherm with a critical point at $G = -\frac{4}{9}$. The initial density is constant except for a randomly distributed small perturbation.

One feature of the free-energy approach is that one can parameterize the free energy to simulate complicated fluid flows, including lamellar fluids. In their study, Gonnella et al (1997) used the following Ginzburg-Landau potential for the ψ function in Equation 43 based on the order parameter, ϕ: $\psi = \frac{\lambda}{2}\phi^2 + \frac{\theta}{4}\phi^4$. They included high-order gradients in the W function: $W = \frac{\kappa}{2}(\nabla\phi)^2 + \frac{\zeta}{2}(\nabla^2\phi)^2$ where θ and ζ are positive. $\lambda < 0$ and $k < 0$ lead to lamellar phases. The magnitude of ζ is directly connected to the elasticity of
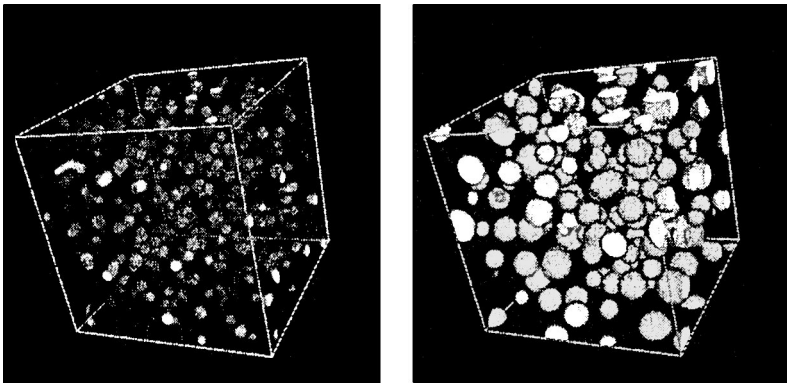

Figure 3   Condensation and subsequent coalescence of liquid drops in supersaturated vapor. Early, *left*, late, *right* (Shan 1997).
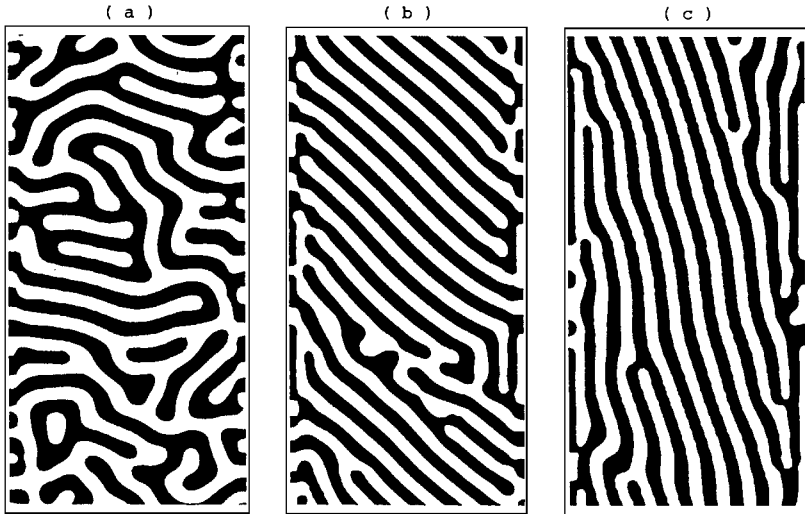
Figure 4   Configuration of a lamellar fluid when a shear flow is applied. The shear velocities are $v = 0$ (*a*), $v = 0.1$ (*b*), and $v = 0.3$ (*c*) (Gonnella et al 1997).

the fluid. In Figure 4, we present flow patterns for a lamellar fluid under a shear induced by forcing a constant velocity v in the left and $-v$ in the right simulation domains, respectively. As the shear was applied, ordered lamellae quickly formed, aligned at an angle to the direction of shear. A further increase of the shear rate resulted in a decrease in the angle between the direction of the lamellae and that of the shear. This pattern directly reflects the balance between the shear force and elastic force of the lamellar fluids. It would be of great interest to use this model for simulating bio-fluids where elasticity is important.

Lattice Boltzmann multiphase fluid models have been extensively used to simulate multicomponent flow through porous media in order to understand the fundamental physics associated with enhanced oil recovery, including relative permeabilities (Vangenabeek et al 1996). The LBM is particularly useful for this problem because of its capability of handling complex geometrical boundary conditions and varying physical parameters, including viscosities (Grunau et al 1993) and wettabilities (Blake et al 1995). In the work by Buckles et al (1994), Martys & Chen (1995), and Ferreol & Rothman (1995), realistic sandstone geometries from oil fields were used. Very complicated flow patterns were observed. The numerical values of the relative permeability as a function of percent saturation of wetting fluid agree qualitatively with experimental data.
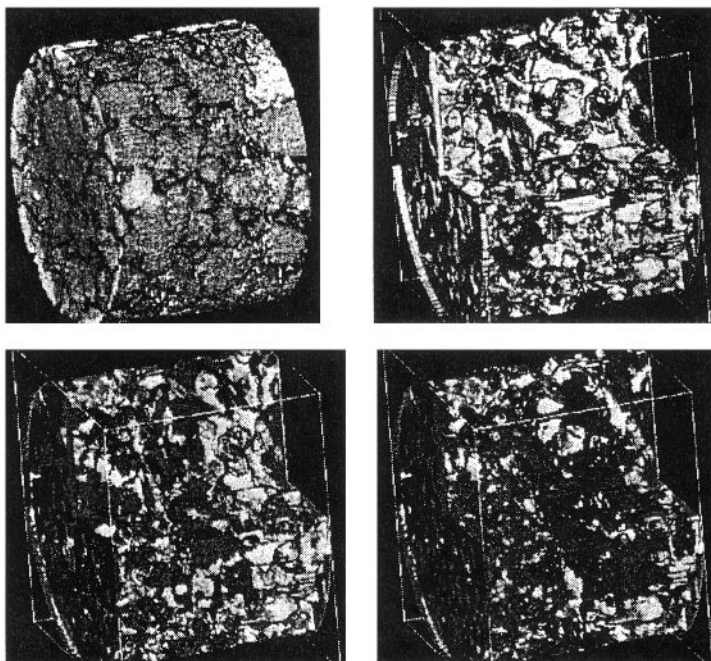
Figure 5   A sandstone sample used in the multiphase LBM simulation (*top left*). Other panels display two-phase fluid flows through the sandstone at different times (Buckles et al 1994).

Gunstensen & Rothman (1993) studied the linear and nonlinear multicomponent flow regimes corresponding to large and small flow rates, respectively. They found, for the first time, that the traditional Darcy's law must be modified in the nonlinear regime because of the capillary effect. Figure 5 shows a typical pore geometry (*top left*). It is a portion of a sandstone sample obtained from a Mobil offshore oil reservoir. Two-phase fluid flows through the sandstone are displayed at successive times (*top right*, *bottom left*, *bottom right*). The sandstone is transparent. The dark color indicates invading water and the grey color indicates oil. As seen in the plot, the lattice Boltzmann simulation preserves the fundamental phenomena observed in experiments that the water phase forms long fingers through the porous medium because of the wettability properties of the water. The LBM is becoming an increasingly popular means of modeling multiphase fluid flows in porous media because of its ability to simulate the exact Navier-Stokes equation in a parallel fashion, to handle complicated geometry, and to simulate surface dynamics and wettability (or contact angles).

LATTICE BOLTZMANN SIMULATION
OF PARTICLES IN FLUIDS

To simulate particles suspended in fluids, an approximate treatment of fluid-particle interaction must be incorporated. Much of the pioneering work and some interesting applications in this area were carried out by Ladd (1993, 1994a,b, 1997). Important variations and applications were mostly associated with Behrend (1995) and Aidun & Lu (1995).

In the model of Ladd, a solid boundary was mapped onto the lattice and a set of boundary nodes, $\mathbf{r}_b$, was defined in the middle of links, whose interior points represent a particle. A no-slip boundary condition on the moving particle requires the fluid velocity to have the same speed at the boundary nodes as the particle velocity $\mathbf{u}_b$ which has the translational part $\mathbf{U}$, and the rotational part Ω_b. Assuming that the center position of the particle is $\mathbf{R}$, then, $\mathbf{u}_b = \mathbf{U} + \Omega_b \times (\mathbf{r}_b - \mathbf{R})$. The distribution function f_i is defined for grid points inside and outside the particle. To account for the momentum change when $\mathbf{u}_b$ was not zero, Ladd proposed adding a term to the distribution function for both sides of the boundary nodes:

$$f_i'(\mathbf{x}) = f_i(\mathbf{x}) \pm B(\mathbf{e}_i \cdot \mathbf{u}_b), \tag{46}$$

where B is a coefficient proportional to the mass density of the fluid and depends on the detailed lattice structure; the $+$ sign applies to boundary nodes at which the particle is moving toward the fluid and $-$ for moving away from the fluid. Equation 46 includes a mass exchange between the fluid inside and the fluid outside the particle. Aidun & Lu (1995) modified Equation 46 by adding an extra term that forces mass conservation for the fluid inside the particle. The details of the boundary rule and variations were studied extensively by Behrend (1995), who improved the efficiency of the algorithm used by Ladd while retaining similar accuracy for translational motion, although the rotational motion is less accurate.

The approximations used so far to simulate moving boundaries are computationally convenient and efficient. In fact, the work for simulating N particles in Ladd's scheme scales linearly with N, in contrast to finite-element schemes, which scale as N^2 (Hu 1996) when the exact incompressible condition is being enforced. The accuracy of the scheme was carefully and extensively studied for creeping flows and flows at finite Reynolds numbers (Ladd 1994b). It compared well with finite-difference and finite-element methods. The drag coefficient of a circular particle in a 2-D channel with gravitational field and the settling trajectory compared well with results from traditional numerical methods and the solution of the Stokes equation (Aidun & Lu 1996).

In the LBM, fluctuations in the distribution functions are ignored. These fluctuations are important for the study of Brownian motion and other effects. To include the fluctuations in the fluid necessary to drive Brownian motion, Dufty & Ernst (1996) and Ladd (1993) added stochastic terms to the distribution function. These distribution function fluctuations are constrained to conserve mass and momentum, but they contribute a fluctuating part to the stress tensor of the fluid. The variance of the stress-tensor fluctuations is related to the effective temperature and the viscosity of the fluid via the fluctuation-dissipation theorem. This method allows—apparently for the first time—treatment of the Brownian short-time regime and the pre-Brownian time regime. Close quantitative agreement is found between experiment and the fluctuating LBM in the short-time regime (Segre et al 1995). Ladd, using up to 32,000 suspended particles in the fluctuation LBM, showed that "there is no evidence that the long-range hydrodynamic interactions are screened by changes in the pair correlation function at large distances." His results leave open the explanation of the experimentally reported absence of the theoretically expected divergence of velocity fluctuations (Ladd 1997).

SIMULATION OF HEAT TRANSFER AND REACTION-DIFFUSION

The lattice Bhatnagar-Gross-Krook (LBGK) models for thermal fluids have been developed by several groups. To include a thermal variable, such as temperature, Alexander et al (1993b) used a two-dimensional 13-velocity model on the hexagonal lattice. In this work, the internal energy per unit mass E was defined through the second-order moment of the distribution function, $\rho E = \sum_{\sigma,i} f_{\sigma,i} (\mathbf{e}_{\sigma,i} - \mathbf{u})^2 / 2$. Here the index $\sigma = 0, 1$, and 2, indicates velocity magnitudes. To have a consistent compressible hydrodynamic equation, the collision operator $\Omega_{\sigma,i}$ was chosen to satisfy local energy conservation: $\sum_i \Omega_{\sigma,i} \mathbf{e}_{\sigma,i}^2 / 2 = 0$, and the third-order velocity dependent terms, such as $(\mathbf{e}_{\sigma,i} \cdot \mathbf{u})^3$, $(\mathbf{e}_{\sigma,i} \cdot \mathbf{u}) u^2$ and u^3, had been included in the equilibrium distribution (Equation 21). The transport coefficients, including viscosity and heat conductivity derived from the Chapman-Enskog expansion, agreed well with numerical simulation. A Couette flow with a temperature gradient between two parallel planes was also simulated and the results agreed well with theoretical predictions when the temperature difference was small. Vahala et al (1995) examined this model by studying the effect of 2-D shear velocity turbulence on a steep temperature gradient profile. Qian (1993) developed 3-D thermal LBM models based on 21 and 25 velocities. Chen et al (1994) extended the above thermal models by including more speeds based on general square lattices in

D dimensions. They utilized the freedom in the equilibrium distribution to eliminate nonphysical high-order effects (Qian & Orszag 1993). Because the multispeed BGK collision operator constrained the momentum and the thermal modes to relax at the same speed, the Prandtl number was fixed. The inclusion of additional properties to provide variation of the Prandtl number was studied by Chen et al (1995) and McNamara et al (1995).

Two limitations in multispeed LBM thermal models severely restrict their application. First, because only a small set of velocities is used, the variation of temperature is small. Second, all existing LBM models suffer from numerical instability (McNamara et al 1995), owing to the absence of an H-theorem. It seems that the numerical instability is more severe in the thermal LBM models than in the isothermal models. Both problems can be partially resolved if one treats the temperature equation as an active scalar and solves it using the relaxation method by adding an independent distribution function (Bartoloni et al 1993). On the other hand, it is difficult for the active scalar approach to incorporate the correct and full dissipation function. Two-dimensional Rayleigh-Bénard (RB) convection was simulated using this active scalar scheme for studying scaling laws (Bartoloni et al 1993) and probability density functions (Massaioli et al 1993) at high Prandtl numbers. Two-dimensional free-convective cavity flow was also simulated (Eggels & Somers 1995), and the results compared well with benchmark data. Two-D and 3-D Rayleigh-Bénard convections were carefully studied by Shan (1997) using a passive scalar temperature equation and a Boussinesq approximation. This scalar equation was derived based on the two-component model of Shan & Chen (1993). The calculated critical Rayleigh number for the RB convection agreed well with theoretical predictions. The Nusselt number as a function of Rayleigh number for the 2-D simulation was in good agreement with previous numerical simulation using other methods.

The LBM was extended by Dawson et al (1993) to describe a set of reaction-diffusion equations advected by velocities governed by the Navier-Stokes equation. They studied hexagonal patterns and stripe patterns caused by the Turing instability in the Selkov model. The effect of fluid flows on the chemical reaction at solid surfaces was simulated (Chen et al 1995) to study geochemical processes, including dissolution and precipitation on rock surfaces and chimney structures at seafloor hydrothermal vents. A similar study on the effect of nutrient diffusion and flow on coral morphology was carried out by Kaandorp et al (1996). Alvarez-Ramirez et al (1996) used the model of Dawson et al (1993) to study the effective diffusivity of a heterogeneous medium when the inclusion was impermeable or permeable with a different diffusivity. They found that the LBM simulation results compared well with Monte Carlo simulations and

agreed well with the predictions using Maxwell's equation. Holme & Rothman (1992) carried out a study of viscous fingering in two-dimensional Hele-Shaw patterns with Péclet number $= 1700$. Creeping flow in a Hele-Shaw cell was also simulated by Flekkøy et al (1996) to investigate the inertial effect at very small Reynolds number, which is sensitive to effects of hydrodynamic irreversibility. Anomalous diffusion of LBM fluids in fractal media and Taylor hydrodynamic dispersion in a two-dimensional channel were simulated by Cali et al (1992). They found that the diffusion scaling exponents agreed well with the exact solution for a Sierpinski gasket. The measured longitudinal diffusion coefficient as a function of flow speed in 2-D Taylor hydrodynamic dispersion agreed well with an asymptotic prediction. This research demonstrates that the LBM is capable of simulating the diffusion process in irregular geometries. The effects of turbulent mixing behind a wake on Turing patterns were studied by Weimar & Boon (1996). They found that the mixing caused by turbulence increased eddy diffusivity and destroyed the pattern formation. Qian et al (1995) simulated front dynamics and scaling properties for the irreversible reaction: $A + B \rightarrow C$.

CONCLUDING REMARKS

This review is intended to be an overview of the subject of the lattice Boltzmann method and its applications in fluid mechanics. The LBM is so diverse and interdisciplinary that it is not possible to include all interesting topics. We refer readers to related review articles written by Benzi et al (1992), Rothman & Zaleski (1994), Chen et al (1995), and Qian et al (1995).

We have introduced the fundamentals of the lattice Boltzmann method, including the lattice Boltzmann equation and its relation to the macroscopic Navier-Stokes equation. Some LBM methods, including multiphase LBM models and fluid-particle interaction models, have been discussed in detail. We have demonstrated that simulation results from the lattice Boltzmann methods are in good quantitative agreement with experimental results and results from other numerical methods.

We wish to emphasize the kinetic nature of the LBM. Because the LBM is a mesoscopic and dynamic description of the physics of fluids, it can model problems wherein both macroscopic hydrodynamics and microscopic statistics are important. The LBM can be considered to be an efficient numerical method for computational fluid dynamics. It is also a powerful tool for modeling new physical phenomena that are not yet easily described by macroscopic equations.

From a computational point of view, the lattice Boltzmann equation is hyperbolic and can be solved locally, explicitly, and efficiently on parallel computers.

Not only is the scheme computationally comparable with traditional numerical methods, but it is also easy to program and to include new physics because of the simplicity of the form of the LBM equations.

The lattice Boltzmann method is still undergoing development. Many models, including simulation of granular flows (Flekkøy & Herrmann 1993, Tan et al 1995), viscoelastic flows (Aharonov & Rothman 1993), magnetohydrodynamics (Martinez et al 1994), and microemulsions (Boghosian et al 1996) were recently proposed. Although innovative and promising, these existing LBM methods, including multicomponent LBM models, require additional benchmarking and verification. The current lattice models for multiphase and reacting systems are most suitable for isothermal problems. The development of a reliable LBM for thermal systems will allow the simulation of heat transfer and surface phenomena simultaneously (Kato 1997). This would open many new areas of application.

Visit the *Annual Reviews home page* at
http://www.AnnualReviews.org.

Literature Cited

Abe T. 1997. Derivation of the lattice Boltzmann method by means of the discrete ordinate method for the Boltzmann equation. *J Comp. Phys.* 131:241–46

Aharonov E, Rothman DH. 1993. Non-Newtonian flow (through porous media): a lattice Boltzmann method. *Geophys. Res. Lett.* 20:679–82

Aidun CK, Lu Y-N. 1995. Lattice Boltzmann simulation of solid particles suspended in fluid. *J. Stat. Phys.* 81:49–61

Alexander FJ, Chen S, Grunau DW. 1993a. Hydrodynamic spinodal decomposition: growth kinetics and scaling. *Phys. Rev. B* 48:634–37

Alexander FJ, Chen S, Sterling JD. 1993b. Lattice Boltzmann thermohydrodynamics. *Phys. Rev. E* 47:R2249–52

Alvarez-Ramirez J, Nieves-Mendoza S, Gonzalez-Trejo J. 1996. Calculation of the effective diffusivity of heterogeneous media using the lattice Boltzmann method. *Phys. Rev. E* 53:2298–2303

Amati G, Succi S, Benzi R. 1997. Turbulent channel flow simulation using a coarse-grained extension of the lattice Boltzmann method. *Fluid Dyn. Res.* 19:289–302

Ancona MG. 1994. Fully-Lagrangian and lattice-Boltzmann methods for solving systems of conservation equations. *J. Comp. Phys.* 115:107–20

Bartoloni A, Battista C, Cabasino S, Paolucci PS, Pech J, et al. 1993. LBE simulations of Rayleigh-Bernard convection on the APE100 parallel processor. *Int. J. Mod. Phys. C* 4:993–1006

Behrend O. 1995. Solid-fluid boundaries in particle suspension simulations via the lattice Boltzmann method. *Phys. Rev. E* 52:1164–75

Benzi R, Succi S. 1990. Two-dimensional turbulence with the lattice Boltzmann equation. *J. Phys. A* 23:L1–5

Benzi R, Succi S, Vergassola M. 1992. The lattice Boltzmann-equation—theory and applications. *Phys. Rep.* 222:145–97

Benzi R, Struglia MV, Tripiccione R. 1996. Extended self-similarity in numerical simula-

tions of three-dimensional anisotropic turbulence. *Phys. Rev. E* 53:R5565–68

Bhatnagar PL, Gross EP, Krook M. 1954. A model for collision processes in gases. I: small amplitude processes in charged and neutral one-component system. *Phys. Rev.* 94:511–525

Blake TD, Deconinck J, Dortona U. 1995. Models of wetting: immiscible lattice Boltzmann automata versus molecular kinetic theory. *Langmuir.* 11:4588–92

Boghosian BM, Coveney PV, Emerton AN. 1996. A lattice-gas model for microemulsions. *Proc. Roy. Soc. London. Ser. A* 452:1221–50

Brackbill JU, Kothe DB, Zemach C. 1992. A continuum method for modeling surface tension. *J. Comp. Phys.* 100:335–54

Broadwell JE. 1964. Study of rarefied shear flow by the discrete velocity method. *J. Fluid Mech.* 19:401–14

Buckles J, Hazlett R, Chen S, Eggert KG, Grunau DW, Soll WE. 1994. Flow through porous media using lattice Boltzmann method. *Los Alamos Sci.* 22:112–21

Cali A, Succi S, Cancelliere A, Benzi R, Gramignani M. 1992. Diffusion and hydrodynamic dispersion with the lattice Boltzmann method. *Phys. Rev. A* 45:5771–74

Cao N, Chen S, Jin S, Martinez D. 1997. Physical symmetry and lattice symmetry in lattice Boltzmann method. *Phys. Rev. E* 55:R21–24

Chang YC, Hou TY, Merriman B, Osher S. 1996. A level set formulation of Eulerian interface capturing methods for incompressible fluid flows. *J. Comp. Phys.* 124:449–64

Chen H. 1993. Discrete Boltzmann systems and fluid flows. *Comp. Phys.* 7:632–37

Chen H, Chen S, Matthaeus WH. 1992. Recovery of the Navier-Stokes equations using a lattice-gas Boltzmann method. *Phys. Rev. A.* 45:R5339–42

Chen S, Chen HD, Martinez D, Matthaeus W. 1991. Lattice Boltzmann model for simulation of magnetohydrodynamics. *Phys Rev. Lett.* 67:3776–79

Chen S, Dawson SP, Doolen GD, Janecky DR, Lawniczak A. 1995. Lattice methods and their applications to reacting systems. *Comp. Chem. Eng.* 19:617–46

Chen S, Lookman T. 1995. Growth kinetics in multicomponent fluids. *J. Stat. Phys.* 81:223–35

Chen S, Martinez D, Mei R. 1996. On boundary conditions in lattice Boltzmann methods. *Phys. Fluids* 8:2527–36

Chen S, Wang Z, Shan XW, Doolen GD. 1992. Lattice Boltzmann computational fluid dynamics in three dimensions. *J. Stat. Phys.* 68:379–400

Chen Y, Ohashi H, Akiyama M. 1994. Thermal lattice Bhatnagar-Cross-Krook model without nonlinear deviations in macrodynamic equations. *Phys. Rev. E* 50:2776–83

Chen Y, Ohashi H, Akiyama M. 1995. Prandtl number of lattice Bhatnagar-Gross-Krook fluid. *Phys. Fluids* 7:2280–82

Chu CK. 1965. Kinetic-Theoretic description of the formation of a shock wave. *Phys. Fluids* 8:12–21

Cieplak M. 1995. Rupture and coalescence in 2-dimensional cellular-automata fluids. *Phys. Rev. E* 51:4353–61

Cornubert R, d'Humières D, Levermore D. 1991. A Knudsen layer theory for lattice gases. *Physica D* 47:241–59

Dawson SP, Chen S, Doolen GD. 1993. Lattice Boltzmann computations for reaction-diffusion equations. *J. Chem. Phys.* 98:1514–23

d'Humières D, Lallemand P, Frisch U. 1986. Lattice gas model for 3D hydrodynamics. *Europhys. Lett.* 2:291–97

D'ortona U, Salin D, Cieplak M, Banavar JR. 1994. Interfacial phenomena in Boltzmann cellular automata. *Europhys. Lett.* 28:317–22

Dufty JW, Ernst MH. 1996. Lattice Boltzmann-Langevin equation. *Fields Inst. Comm.* 6:99–107

E W-N, Liu J-G. 1996. Essentially compact scheme for unsteady viscous incompressible flows. *J. Comp. Phys.* 126:122–38

Eggels JGM. 1996. Direct and large-eddy simulation of turbulent fluid flow using the lattice-Boltzmann scheme. *Int. J. Heat Fluid Flow* 17:307–23

Eggels JGM, Somers JA. 1995. Numerical simulation of free convective flow using the lattice-Boltzmann scheme. *J. Heat Fluid Flow* 16:357–64

Elton BH, Levermore CD, Rodrigue H. 1995. Covergence of convective-diffusive lattice Boltzmann methods. *SIAM J. Sci. Comp.* 32:1327–54

Ferreol B, Rothman DH. 1995. Lattice-Boltzmann simulations of flow-through Fontainebleau sandstone. *Transp. Por. Med.* 20:3–20

Flekkøy EG, Herrmann HJ. 1993. Lattice Boltzmann models for complex fluids. *Physica A.* 199:1–11

Flekkøy EG, Rage T, Oxaal U, Feder J. 1996. Hydrodynamic irreversibility in creeping flow. *Phys. Rev. Lett.* 77:4170–73

Frisch U, Hasslacher B, Pomeau Y. 1986. Lattice-gas automata for the Navier-Stokes equations. *Phys. Rev. Lett.* 56:1505–8

Frisch U, d'Humiéres D, Hasslacher B, Lallemand P, Pomeau Y, Rivet J-P. 1987. Lattice gas hydrodynamics in two and three dimensions. *Complex Syst.* 1:649–707

Ginzbourg I, Adler PM. 1994. Boundary flow condition analysis for the three-dimensional lattice Boltzmann model. *J. Phys. II* 4:191–214

Glimm JE, Issacson E, Marchesin D, McBryan O. 1981. Front tracking for hyperbolic systems. *Adv. Appl. Math.* 2:91–119

Gonnella G, Orlandini E, Yeomans JM. 1997. Spinodal decomposition to a lamellar phase: effects of hydrodynamic flow. *Phys. Rev. Lett.* 78:1695–98

Grunau D, Chen S, Eggert K. 1993. A lattice Boltzmann model for multiphase fluid flows. *Phys. Fluids A* 5:2557–62

Gunstensen AK, Rothman DH. 1993. Lattice Boltzmann studies of immiscible two phase flow through porous media *J. Geophys. Res.* 98:6431–41

Gunstensen AK, Rothman DH, Zaleski S, Zanetti G. 1991. Lattice Boltzmann model of immiscible fluids. *Phys. Rev. A*. 43:4320–27

Hardy J, de Pazzis O, Pomeau Y. 1976. Molecular dynamics of a classical lattice gas: transport properties and time correlation functions. *Phys. Rev. A* 13:1949–61

Hayot F, Wagner L. 1996. A non-local modification of a lattice Boltzmann model. *Europhys. Lett.* 33:435–40

He X, Doolen GD. 1997. Lattice Boltzmann method on curvilinear coordinates system: vortex shedding behind a circular cylinder. *Phys. Rev. E.* In press

He X, Luo L-S. 1997. A priori derivation of the lattice Boltzmann equation. *Phys. Rev. E.* 55:6333–36

He X, Luo L-S, Dembo M. 1996. Some progress in lattice Boltzmann method. Part I nonuniform mesh grids. *J. Comp. Phys.* 129:357–63

He X, Zou Q, Luo L-S, Dembo M. 1997. Analytic solutions of simple flow and analysis of non-slip boundary conditions for the lattice Boltzmann BGK model. *J. Stat. Phys.* 87:115–36

Heijs AWJ, Lowe CP. 1995. Numerical evaluation of the permeability and the Kozeny constant for two types of porous media. *Phys. Rev. E* 51:4346–52

Higuera FJ, Jiménez J. 1989. Boltzmann approach to lattice gas simulations. *Europhys. Lett.* 9:663–68

Higuera FJ, Succi S. 1989. Simulating the flow around a circular cylinder with a lattice Boltzmann equation. *Europhys. Lett.* 8:517–21

Higuera FJ, Succi S, Benzi R. 1989. Lattice gas dynamics with enhanced collisions. *Europhys. Lett.* 9:345–49

Holme R, Rothman DH. 1992. Lattice-gas and lattice-Boltzmann models of miscible fluids. *J. Stat. Phys.* 68:409–29

Hou S. 1995. *Lattice Boltzmann method for incompressible viscous flow.* PhD thesis. Kansas State Univ., Manhattan, Kansas

Hou S, Zou Q, Chen S, Doolen G, Cogley AC. 1995. Simulation of cavity flow by the lattice Boltzmann method. *J. Comp. Phys.* 118:329–47

Hou S, Sterling J, Chen S, Doolen GD. 1996. A lattice Boltzmann subgrid model for high Reynolds number flows. *Fields Inst. Comm.* 6:151–66

Hu HH. 1996. Direct simulation of flows of solid-liquid mixtures. *Int. J. Multiphase flow.* 22:335–52

Inamuro T, Sturtevant B. 1990. Numerical study of discrete-velocity gases. *Phys. Fluids* 2:2196–2203

Inamuro T, Yoshino M, Ogino F. 1995. A non-slip boundary condition for lattice Boltzmann simulations. *Phys. Fluids* 7:2928–30

Jin S, Katsoulakis M. Relaxation approximations to front propagation. *J. Diff. Eq.* In press

Jin S, Xin ZP. 1995. The relaxation schemes for systems of conservation laws in arbitrary space dimensions. *Comm. Pure Appl. Math.* 48:235–76

Kaandorp JA, Lowe CP, Frenkel D, Sloot PMA. 1996. Effect of nutrient diffusion and flow on coral morphology. *Phys. Rev. Lett.* 77:2328–31

Kadanoff L. 1986. On two levels. *Phys. Today* 39:7–9

Kato T, Kono K, Seta K, Martinez D, Chen S. 1997. Boiling two-phase flow by the lattice Boltzmann method *Int. J. Mod. Phys.* In press

Kim J, Moin P, Moser R. 1987. Turbulence statistics in fully-developed channel flow at low Reynolds number. *J. Fluid Mech.* 177:133–66

Koelman JMVA. 1991. A simple lattice Boltzmann scheme for Navier-Stokes fluid flow. *Europhys. Lett.* 15:603–7

Koplik J, Lasseter T. 1985. One- and two-phase flow in network models of porous media. *Chem. Eng. Comm.* 26:285–95

Kraichnan RH. 1967. Inertial ranges in two-dimensional turbulence. *Phys. Fluids* 10:1417–23

Ladd AJ. 1993. Short-time motion of colloidal particles: numerical simulation via a fluctuating lattice-Boltzmann equation *Phys. Rev. Lett.* 70:1339–42

Ladd AJC. 1994a. Numerical simulations of particulate suspensions via a discretized Boltzmann equation. Part. 1. theoretical foundation. *J. Fluid Mech.* 271:285–309

Ladd AJC. 1994b. Numerical simulations of particulate suspensions via a discretized Boltzmann equation. Part 2: Numerical results. *J. Fluid Mech.* 271:311–39

Ladd AJC. 1997. Sedimentation of homoge-

neous suspensions of non-Brownian spheres *Phys. Fluids* 9:491–99

Laudau LD, Lifshitz EM. 1959. *Fluid Dyn.* New York: Pergamon

Lavallée P, Boon JP, Noullez A. 1991. Boundaries in lattice gas flows. *Physica D* 47:233–40

Luo L. 1997. Symmetry breaking of flow in 2-D symmetric channels: simulations by lattice Boltzmann method. *Int. J. Mod. Phys. C.* In press

Maier RS, Bernard RS, Grunau DW. 1996. Boundary conditions for the lattice Boltzmann method. *Phys. Fluids* 8:1788–1801

Majda A. 1984. *Compressible Fluid and Systems of Conservation Laws in Several Space Variables.* New York: Springer-Verlag

Martys NS, Chen H. 1996. Simulation of multicomponent fluids in complex three-dimensional geometries by the lattice Boltzmann method. *Phys. Rev. E* 53:743–50

Martinez DO, Chen S, Matthaeus WH. 1994. Lattice Boltzmann magnetohydrodynamics. *Phys. Plasmas* 1:1850–67

Martinez DO, Matthaeus WH, Chen S, Montgomery DC. 1994. Comparison of spectral method and lattice Boltzmann simulations of two-dimensional hydrodynamics. *Phys. Fluids* 6:1285–98

Massaioli F, Benzi R, Succi S. 1993. Exponential tails in two-dimensional Rayleigh-Bénard convection. *Europhys. Lett.* 21:305–10

McNamara GR, Garcia AL, Alder BJ. 1995. Stabilization of thermal lattice Boltzmann models. *J. Stat. Phys.* 81:395–408

McNamara GR, Zanetti G. 1988. Use of the Boltzmann equation to simulate lattice-gas automata. *Phys. Rev. Lett.* 61:2332–35

Miller W. 1995. Flow in the driven cavity calculated by the lattice Boltzmann method. *Phys. Rev. E* 51:3659–69

Nadiga BT. 1995. An Euler solver based on locally adaptive discrete velocities. *J. Stat. Phys.* 81:129–46

Nadiga BT, Pullin DI. 1994. A method for near-equilibrium discrete-velocity gas flows. *J. Comp. Phys.* 112:162–72

Nadiga BT, Zaleski S. 1996. Investigations of a two-phase fluid model. *Eur. J. Mech. B/Fluids* 15:885–96

Nannelli F, Succi S. 1992. The lattice Boltzmann-equation on irregular lattices. *J. Stat. Phys.* 68:401–7

Noble DR, Chen S, Georgiadis JG, Buckius RO. 1995. A consistent hydrodynamic boundary condition for the lattice Boltzmann method. *Phys. Fluids* 7:203–9

Noble DR, Georgiadis JG, Buckius RO. 1996. Comparison of accuracy and performance for lattice Boltzmann and finite difference simulations of steady viscous flow. *Int. J. Numer. Meth. Fluids* 23:1–18

Orszag SA, Yakhot V. 1986. Reynolds number scaling of cellular automaton hydrodynamics. *Phys. Rev. Lett.* 56:1691–93

Osborn WR, Orlandini E, Swift MR, Yeomans JM, Banavar JR. 1995. Lattice Boltzmann study of hydrodynamic spinodal decomposition. *Phys. Rev. Lett.* 75:4031–34

Prasad AK, Koseff JR. 1989. Reynolds-number and end-wall effects on a lid-driven cavity flow. *Phys. Fluids A* 1:208–18

Qian YH. 1990. *Lattice gas and lattice kinetic theory applied to the Navier-Stokes equations.* PhD thesis. Université Pierre et Marie Curie, Paris

Qian YH. 1993. Simulating thermohydrodynamics with lattice BGK models. *J. Sci. Comp.* 8:231–41

Qian YH, d'Humières D, Lallemand P. 1992. Lattice BGK models for Navier-Stokes equation. *Europhys. Lett.* 17:479–84

Qian YH, Orszag SA. 1993. Lattice BGK models for the Navier-Stokes equation: nonlinear deviation in compressible regimes. *Europhys. Lett.* 21:255–59

Qian YH, Succi S, Massaioli F, Orszag SA. 1996. A benchmark for lattice BGK model: flow over a backward-facing step. *Fields Inst. Comm.* 6:207–14

Qian YH, Succi S, Orszag SA. 1995. Recent advances in lattice Boltzmann computing. *Annu. Rev. Comp. Phys.* 3:195–242

Rothman DH. 1988. Cellular-automaton fluids: a model for flow in porous media. *Geophys.* 53:509–18

Rothman DH, Keller JM. 1988. Immiscible cellular-automaton fluids. *J. Stat. Phys.* 52:1119–27

Rothman DH, Zaleski S. 1994. Lattice-gas models of phase separation: interfaces, phase transitions and multiphase flow. *Rev. Mod. Phys.* 66:1417–79

Rybka RB, Cieplak M, Salin D. 1995. Boltzmann cellular-automata studies of the spinodal decomposition. *Physica A* 222:105–18

Reider MB, Sterling JD. 1995. Accuracy of discrete-velocity BGK models for the simulation of the incompressible Navier-Stokes equations. *Comput. Fluids* 24:459–67

Schreiber R, Keller HB. 1983. Driven cavity flows by efficient numerical techniques. *J. Comp. Phys.* 49:310–33

Schwarz LM, Martys N, Bentz DP, Garboczi EJ, Torquato S. 1993. Cross-property relations and permeability estimation in model porous media. *Phys. Rev. E* 48:4584–91

Segre PN, Behrend OP, Pusey PN. 1995. Short-time Brownian motion in colloidal suspensions: experiment and simulation. *Phys. Rev. E* 52:5070–83

Shan X. 1997. Simulation of Rayleigh-Bénard convection using a lattice Boltzmann method. *Phys. Rev. E* 55:2780–88

Shan X, Chen H. 1993. Lattice Boltzmann model for simulating flows with multiple phases and components. *Phys. Rev. E* 47:1815–19

Shan X, Chen H. 1994. Simulation of nonideal gases and liquid-gas phase transitions by the lattice Boltzmann equation. *Phys. Rev. E* 49:2941–48

Shan X, Doolen G. 1995. Multicomponent lattice-Boltzmann model with interparticle interaction. *J. Stat. Phys.* 81:379–93

Skordos PA. 1993. Initial and boundary conditions for the lattice Boltzmann method. *Phys. Rev. E* 48:4823–42

Soll W, Chen S, Eggert K, Grunau D, Janecky D. 1994. Applications of the lattice-Boltzmann/lattice gas techniques to multifluid flow in porous media. In *Computational Methods in Water Resources X*, ed. A Peters, pp. 991–99. Dordrecht: Academic

Somers JA. 1993. Direct simulation of fluid flow with cellular automata and the lattice-Boltzmann equation. *Applied Sci. Res.* 51:127–33

Spaid MAA, Phelan FR Jr. 1997. Lattice Boltzmann methods for modeling microscale flow in fibrous porous media. *Phys. Fluids.* 9:2468–74

Sterling JD, Chen S. 1996. Stability analysis of lattice Boltzmann methods. *J. Comp. Phys.* 123:196–206

Swift MR, Osborn WR, Yeomans JM. 1995. Lattice Boltzmann simulation of nonideal fluids. *Phys. Rev. Lett.* 75:830–33

Swift MR, Orlandini SE, Osborn WR, Yeomans JM. 1996. Lattice Boltzmann simulations of liquid-gas and binary-fluid systems. *Phys. Rev. E* 54:5041–52

Succi S, Amati G, Benzi R. 1995. Challenges in lattice Boltzmann computing. *J. Stat. Phys.* 81:5–16

Succi S, Benzi R, Higuera F. 1991. The lattice-Boltzmann equation—a new tool for computational fluid dynamics. *Physica D* 47:219–30

Succi S, Foti E, Higuera F. 1989. Three-dimensional flows in complex geometries with the lattice Boltzmann method. *Europhys. Lett.* 10:433–38

Succi S, Nannelli F. 1994. The finite volume formulation of the lattice Boltzmann equation. *Transp. Theory Stat. Phys.* 23:163–71

Tan M-L, Qian YH, Goldhirsch I, Orszag SA. 1995. Lattice-BGK approach to simulating granular flows. *J. Stat. Phys.* 81:87–103

Treviño C, Higuera F. 1994. Lattice Boltzmann and spectral simulations of non-linear stability of Kolmogorov flows. *Rev. Mex. Fis.* 40:878–90

Vahala G, Pavlo P, Vahala L, Chen H. 1995. Effect of velocity shear on a strong temperature gradient—a lattice Boltzmann approach. *Phys. Lett. A* 202:376–82

Vangenabeek O, Rothman DH. 1996. Macroscopic manifestations of microscopic flows through porous-media phenomenology from simulation. *Annu. Rev. Earth Planet. Sci.* 24:63–87

Vanka SP. 1986. Block-implicit multigrid solution of Navier-Stokes equations in primitive variables. *J. Comp. Phys.* 65:138–58

Wagner L. 1994. Pressure in lattice Boltzmann simulations of flow around a cylinder. *Phys. Fluids* 6:3516–18

Weimar JR, Boon JP. 1996. Nonlinear reactions advected by a flow. *Physica A* 224:207–15

Wolfram S. 1986. Cellular automaton fluids. 1: Basic theory. *J. Stat. Phys.* 45:471–526

Wu Y, Alexander FJ, Lookman T, Chen S. 1995. Effects of hydrodynamics on phase transition kinetics in two-dimensional binary fluids. *Phys. Rev. Lett.* 74:3852–55

Xu K, Prendergast KH. 1994. Numerical Navier-Stokes solutions from gas kinetic theory. *J. Comp. Phys.* 114:9–17

Ziegler DP. 1993. Boundary conditions for lattice Boltzmann simulations. *J. Stat. Phys.* 71:1171–77

Zou Q, He X. 1997. On pressure and velocity boundary conditions for the lattice Boltzmann BGK model. *Phys. Fluids.* 9:1591–98

Zou Q, Hou S, Doolen GD. 1995. Analytical solutions of the lattice Boltzmann BGK model. *J. Stat. Phys.* 81:319–34